A comprehensive numerical model of steady state saltation (COMSALT)

Jasper F. Kok[1,2] and Nilton O. Renno[1,2]

Received 2 January 2009; revised 20 May 2009; accepted 10 June 2009; published 9 September 2009.

[1] The blowing of sand by wind, known as saltation, ejects dust aerosols into the atmosphere, creates sand dunes, and erodes geological features. We present a comprehensive numerical model of steady state saltation (COMSALT) that, in contrast to most previous studies, can reproduce a wide range of measurements and can simulate saltation over mixed soils. COMSALT calculates the motion of saltating particles due to gravity, fluid drag, particle spin, fluid shear, and turbulence and explicitly accounts for the retardation of the wind due to drag from saltating particles. Furthermore, we included a novel physically based parameterization of the ejection of surface particles by impacting saltating particles which matches experimental results. COMSALT is the first numerical saltation model to reproduce measurements of the wind shear velocity at the impact threshold (i.e., the lowest shear velocity for which saltation is possible) and of the aerodynamic roughness length in saltation. It also reproduces a range of other saltation processes, including profiles of the wind speed and particle mass flux, and the size distribution of saltating particles. As such, COMSALT is the first physically based numerical model to reproduce such a wide range of experimental data. Since we use a minimum of empirical relations, COMSALT can be easily adapted to study saltation under a variety of physical conditions, such as saltation on other planets, saltation under water, and saltating snow.

Citation: Kok, J. F., and N. O. Renno (2009), A comprehensive numerical model of steady state saltation (COMSALT), *J. Geophys. Res.*, *114*, D17204, doi:10.1029/2009JD011702.

1. Introduction

[2] A comprehensive understanding of wind-blown sediment transport is essential for a wide range of processes across scientific disciplines. Indeed, wind-blown sand and dust create sand dunes and dune ripples [*Bagnold*, 1941], erode geological features [*Greeley and Iversen*, 1985] and agricultural fields [*Sterk*, 2003], and are a key component of dust storms and dust devils on Earth and Mars [*Shao*, 2000; *Renno et al.*, 2004]. Soil dust emitted by these features substantially affects climate [*Sokolik et al.*, 2001] and provides limiting nutrients to a range of ecosystems [*Jickells et al.*, 2005]. Outside of Earth, the transport of sediment by wind also shapes the landscape on Mars, Venus, and Titan [e.g., *Greeley and Iversen*, 1985], and dust aerosols are of major importance to the Martian climate [*Fenton et al.*, 2007].

[3] As wind speed increases, sand particles of ~70–500 μm diameter are the first to be moved by wind. After lifting, these particles bounce along the surface in a series of hops [*Greeley and Iversen*, 1985; *Shao*, 2000] in a process known as saltation (Figure 1). The impact of these saltating particles on the soil surface can mobilize particles of a wide range of sizes. Indeed, dust particles, defined as particles with diameter <62.5 μm [*Greeley and Iversen*, 1985], are not normally lifted by wind because their cohesive forces are large compared to the forces due to wind stress [*Shao and Lu*, 2000; *Kok and Renno*, 2006]. These small dust particles are instead ejected from the soil through impacts of saltating particles [*Shao et al.*, 1993]. After their ejection, these dust particles can be transported upwards by convection and turbulent eddies and affect the Earth system in a variety of manners as outlined above and in the work of *Goudie and Middleton* [2006].

[4] Saltating particles can also mobilize larger particles. However, the acceleration of particles with diameters in excess of ~500 μm is limited by their large inertia and these particles generally do not enter saltation [*Shao*, 2000]. Instead, they roll or slide along the surface, driven by impacts of saltating particles and direct wind pressure in a mode of transport known as "creep" [*Bagnold*, 1941].

[5] Saltation is initiated when the shear stress τ exerted by wind on the soil surface exceeds the "fluid threshold" τ_t (~0.05 N/m^2 for loose sand) at which surface particles are lifted [*Bagnold*, 1941; *Greeley and Iversen*, 1985; *Shao*, 2000]. These lifted particles undergo ballistic trajectories during which they are accelerated by wind drag. After a few hops, saltating particles can be sufficiently accelerated to eject (or "splash") other particles from the soil [*Bagnold*,

[1]Applied Physics Program, University of Michigan, Ann Arbor, Michigan, USA.
[2]Atmospheric, Oceanic, and Space Sciences, University of Michigan, Ann Arbor, Michigan, USA.

0148-0227/09/2009JD011702

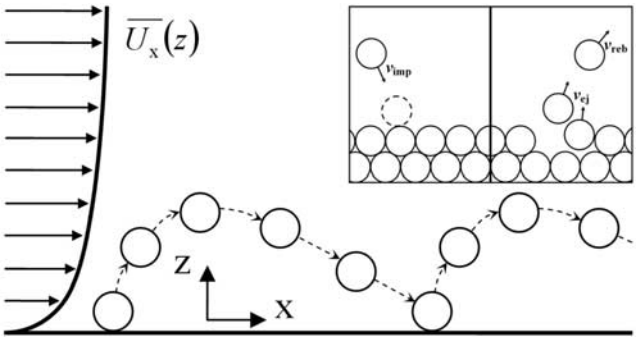

Figure 1. Schematic representation of saltation, showing the logarithmic wind profile $\overline{U}_x(z)$ (see section 2.3) to the left of an idealized spherical sand particle propelled by the wind and bouncing along the surface. After lift-off from the surface, saltating particles gain horizontal momentum from the wind, which is partially converted into vertical momentum after colliding with the surface and rebounding. The inset shows a schematic representation of a saltating particle (left) approaching the soil surface and (right) rebounding from it and ejecting (or "splashing") several surface particles.

1973; *Ungar and Haff*, 1987]. Newly ejected particles are then accelerated by wind and eject more particles when impacting the surface. This causes an exponential increase in the number of saltating particles in the initial stages of saltation [*Anderson and Haff*, 1988, 1991; *Shao and Raupach*, 1992; *McEwan and Willetts*, 1993], after which the momentum fluxes of the fluid and saltating particles reach an equilibrium. This equilibrium is determined by the finite amount of momentum available to be transferred from the wind to the saltating particles, such that the wind profile in the presence of saltation is often substantially reduced from that without saltation [e.g., *Owen*, 1964].

[6] In steady state saltation, surface particles are rarely lifted directly by fluid forces because the wind shear velocity at the surface is lower than the fluid threshold. This subthreshold surface wind shear occurs because the transfer of momentum to the soil surface is dominated by the impacts of saltating particles, not by wind drag [*Bagnold*, 1937, 1973; *Ungar and Haff*, 1987; *Anderson and Haff*, 1988, 1991; *Shao and Raupach*, 1992; *McEwan and Willetts*, 1991, 1993]. As a result, once saltation is initiated, it can be maintained at shear velocities somewhat below the fluid threshold. The minimum shear velocity at which saltation can occur in this manner is termed the "impact threshold" [*Bagnold*, 1941] and, for Earth ambient conditions, is approximately 80–85% of the fluid threshold [*Bagnold*, 1937].

[7] Numerical models of the different physical processes involved in saltation have been developed over the past several decades by various researchers. *White and Schulz* [1977], *Hunt and Nalpanis* [1985], and *Anderson and Hallet* [1986] were the first to successfully model the trajectories of saltating particles. Building on the success of these initial studies, *Ungar and Haff* [1987] were the first to couple the motion of saltating particles to the retardation of the wind speed near the surface in a simple, steady state model, in which the trajectories of all saltating particles were assumed identical. Nonetheless, Ungar and Haff were able to reproduce some essential features of saltation, such as the near-surface focusing of the wind profiles for different shear velocities (first reported by *Bagnold* [1936]). *Werner* [1990] developed a more comprehensive numerical model of steady state saltation that allowed for a range of particle trajectories. This model also included a parameterization of the ejection, or "splashing," of particles from the soil, which was based on laboratory measurements of particle ejections [*Werner*, 1987]. However, only the more detailed models developed by *Anderson and Haff* [1988, 1991] and *McEwan and Willetts* [1991, 1993] were able to simulate the development of saltation from inception to steady state. *Shao and Li* [1999] built on these studies and developed a saltation model as part of a large eddy model that explicitly solved for the wind field. More recently, *Almeida et al.* [2006] coupled a saltation model to the computational fluid dynamics model FLUENT capable of calculating the turbulent wind field in the presence of saltation. While their saltation model assumes identical trajectories and does not explicitly consider the splashing of surface particles, they were able to reproduce empirical expressions for the saltation mass flux. They used this model to study saltation on Mars [*Almeida et al.*, 2008]. Zheng and coworkers also developed a numerical model that can reproduce certain essential features of saltation and were the first to account for the effects of electrostatic forces [*Zheng et al.*, 2006; *Yue and Zheng*, 2006]. The subsequent numerical study of *Kok and Renno* [2008] indicated that electrostatic forces increase the saltating particle concentration [*Kok and Renno*, 2006] and lower the height of saltation trajectories, thereby possibly resolving the discrepancy between the measured [*Greeley et al.*, 1996; *Namikas*, 2003] and predicted [*Bagnold*, 1941; *Owen*, 1964] height of the saltation layer.

[8] While the models discussed above have provided critical advances in our understanding of saltation, they have nonetheless suffered from a number of shortcomings. First, most previous models were restricted to monodisperse soils, while natural saltation takes place over soils that contain a wide range of particle sizes [e.g., *Namikas*, 2003, 2006]. Second, while some of the models discussed above have been able to reproduce specific processes in saltation, no model has yet been able to correctly reproduce a wide range of measurements of natural saltation.

[9] To remedy these problems, we present the most comprehensive physically based numerical model of saltation to date, which we term "COMSALT." Our model includes many of the advances of previous models and in addition includes (1) a physically based parameterization of the splashing of surface particles that agrees with experimental and numerical studies, (2) a generalization of this splashing process to beds of mixed particle sizes, and (3) a detailed treatment of the influence of turbulence on particle trajectories, which agrees with laboratory measurements.

[10] Partially as a result of these improvements, COMSALT can simulate saltation over soils composed of particles of various sizes. Moreover, our model shows reasonable to excellent agreement with a wide range of experimental data, such as horizontal and vertical profiles of particle mass flux, the wind profile in saltation, and the size distribution of saltating particles. Furthermore, COMSALT

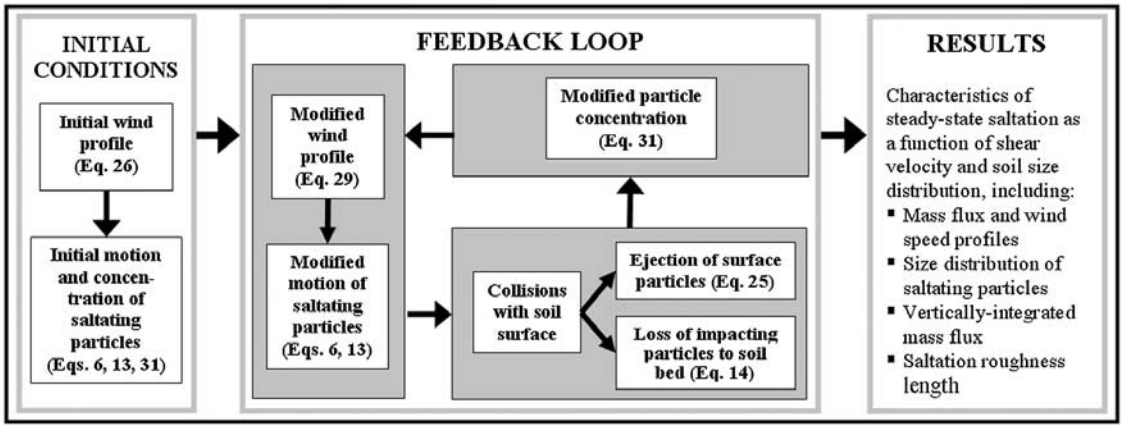

Figure 2. Schematic diagram of our comprehensive numerical model of steady state saltation (COMSALT). As in previous studies [*Anderson and Haff*, 1988, 1991; *Werner*, 1990; *McEwan and Willetts*, 1991, 1993], we model saltation by explicitly simulating (1) particle trajectories, (2) the collision of particles with the soil surface and the subsequent splashing of surface particles into the fluid stream, and (3) the modification of the wind profile through momentum transfer between the wind flow and saltating particles. The model is initiated by aerodynamically lifting several particles with a speed sufficient to reach a few particle diameters [*Anderson and Haff*, 1991], after which the steps in the feedback loop are repeated until the changes in the saltation trajectories, the wind profile, and the particle concentration are smaller than a specified value in successive iterations. Because of the stochastic interaction of saltating particles with the turbulent wind (section 2.1.2) and the soil surface (section 2.2), steady state saltation as simulated by our model is a dynamic balance over longer timescales. This is also characteristic of natural saltation [e.g., *Anderson and Haff*, 1991; *Jackson and McCloskey*, 1997]. The model does not incorporate aerodynamic lifting in steady state saltation, because the fluid shear stress at the surface is below the threshold for lifting (see section 1). For computational efficiency, the model explicitly simulates the trajectories of only a fraction of the particles and considers those representative of the entire ensemble of saltating particles. Increasing this fraction does not significantly alter the results presented here.

is the first model to reproduce measurements of the impact threshold and the aerodynamic roughness length in saltation. To the best of our knowledge, COMSALT is the first physically based model capable of reproducing such a wide range of experimental data. Since we use a minimum of empirical relations, we argue that COMSALT can accurately simulate saltation in a variety of physical environments, including saltating snow [*Nemoto and Nishimura*, 2004], saltation in water, and saltation on other planets such as Mars [*Renno and Kok*, 2008; *Almeida et al.*, 2008; *Kok and Renno*, 2009]. COMSALT was coded in MATLAB and is freely available by contacting the first author (J.K.).

[11] We describe COMSALT in detail in section 2, compare its results to measurements in section 3, and present conclusions in section 4.

2. Model Description

[12] We model steady state saltation as the interplay of several processes (see Figure 2): (1) the motion of saltating particles, (2) the modification of the wind profile through momentum transfer between the wind flow and saltating particles, and (3) the collision of particles with the soil surface and the subsequent splashing of surface particles into the fluid stream [*Werner*, 1990; *Anderson and Haff*, 1991; *McEwan and Willetts*, 1991]. For simplicity, we simulate particle motion in two dimensions, as previous investigators have also done [e.g., *Werner*, 1990; *Anderson and Haff*, 1991; *McEwan and Willetts*, 1991]. We also neglect the collisions of saltating particles with each other, as well as the effects of electrostatic forces, which are generated through "triboelectrification" [*Kok and Lacks*, 2009], on particle trajectories [*Kok and Renno*, 2006, 2008]. The effect of both these processes is limited for small to medium shear velocities (i.e., $u^* < \sim 0.5$ m/s) but probably becomes important for larger shear velocities [*Kok and Renno*, 2008; *Sorensen and McEwan*, 1996; *Huang et al.*, 2007]. We therefore plan to include both midair collisions and electrostatic forces in a future model version (J. F. Kok and N. O. Renno, manuscript in preparation, 2009).

[13] COMSALT uses the logarithmic wind profile known as the "law of the wall" [*Prandtl*, 1935] to calculate the initial trajectories of saltating particles. The drag exerted by the particles on the wind is then obtained from these trajectories and used to adjust the wind profile. The concentration of saltating particles is calculated using the steady state condition that the number of particles striking the soil must be equal to the number of rebounding and ejected particles. If the number of rebounding and ejected particles is greater than the number of impacting particles, then the concentration of saltating particles is increased accordingly, which enhances the exchange of momentum with the wind and reduces the near-surface wind speed, causing particles to strike the soil at reduced speed and thereby eject fewer

particles. Because of their interdependence, the particle concentration, wind profile, and particle trajectories are calculated iteratively until steady state is reached (see Figure 2). Because the interaction of saltating particles with the soil surface and the turbulent wind is stochastic (see sections 2.1.2 and 2.2), these processes cause variability in the model simulations that can be seen as characteristic of natural saltation. "Steady state" saltation as simulated by our model thus entails a dynamic balance that, averaged over many iterations, satisfies the condition that the number of impacting particles is equal to the number of particles that rebound and are ejected from the soil [*Jackson and McCloskey*, 1997; *Anderson and Haff*, 1991].

[14] We discuss each component of the model in detail below. Where possible, we use experimental data to verify the performance of individual model components.

2.1. Particle Trajectories

[15] The motion of saltating particles is determined mainly by gravitational and fluid forces. For the present model version, we thus neglect electrostatic forces [*Kok and Renno*, 2008] and midair collisions [*Sorensen and McEwan*, 1996; *Dong et al.*, 2005; *Huang et al.*, 2007] which affect particle trajectories mostly for large shear velocities.

2.1.1. Fluid Forces

[16] The main fluid force affecting particle trajectories is the drag force [e.g., *Anderson and Haff*, 1991],

$$F_{\mathrm{d}} = -\frac{\pi D_{\mathrm{p}}^2}{8}\rho_{\mathrm{a}} C_{\mathrm{d}} v_{\mathrm{R}} \mathbf{v_R}, \tag{1}$$

where D_{p} is the diameter of a sphere with the same volume as the irregularly shaped sand particle, ρ_{a} is the air density, $\mathbf{v_R} = \mathbf{v} - \mathbf{U}$ is the difference between the particle ($\mathbf{v}$) and wind ($\mathbf{U}$) velocities, and $v_{\mathrm{R}} = |\mathbf{v_R}|$. The drag coefficient ($C_{\mathrm{d}}$) of natural sand particles is generally larger than that for spherical particles of the same volume, both because their irregular shape produces a larger effective surface area than a sphere and because regions of large curvature can lead to flow separation, which increases the drag [*Dietrich*, 1982]. Detailed measurements of the terminal velocity in water have been used to measure the drag coefficient of natural sand particles [*Dietrich*, 1982; *Camenen*, 2007]. We calculate the drag coefficient of a saltating sand particle using an equation proposed by *Cheng* [1997] that includes the effects discussed above

$$C_{\mathrm{d}} = \left[\left(\frac{32}{\mathrm{Re}}\right)^{2/3} + 1\right]^{3/2}, \tag{2}$$

where the particle Reynolds number is given by

$$\mathrm{Re} = \frac{\rho_{\mathrm{a}} v_{\mathrm{R}} D_{\mathrm{p}}}{\mu}. \tag{3}$$

[17] Saltating particles also experience lift forces both due to the shearing flow (the "Saffman force") [*Saffman*, 1965, 1968] and from particle rotation (the "Magnus force") [*Rubinow and Keller*, 1961]. We calculate these lift forces using the following expressions proposed by *Loth* [2008]:

$$F_{\mathrm{saff}} = 1.615 J^* D_{\mathrm{p}}^2 \left(\rho_{\mathrm{a}}\mu\frac{\partial U_{\mathrm{x}}}{\partial z}\right)^{1/2} (\hat{\mathbf{y}} \times \mathbf{v_R}) \tag{4}$$

and

$$F_{\mathrm{mag}} = \frac{\pi}{8}\rho_{\mathrm{a}} D_{\mathrm{p}}^3 C_{\mathrm{L}\Omega}^* (\mathbf{\Omega}_{\mathrm{p}} \times \mathbf{v}_{\mathrm{R}}), \tag{5}$$

where U_{x} is the horizontal wind speed, $\hat{\mathbf{y}}$ is the unit vector perpendicular to the plane in which particle motion takes place, and J^* is a strong function of the shear of the flow, the kinematic viscosity, and the relative velocity of the particle to the fluid and is defined by *McLaughlin* [1991]. The normalized spin lift coefficient $C_{\mathrm{L}\Omega}^*$ is given by *Loth* [2008, equation (16)] and is $\sim$0.5–0.7 for normal flow conditions in saltation on Earth. Previous studies have often assumed $C_{\mathrm{L}\Omega}^* = 1$, which is a good approximation only for $\mathrm{Re} \ll 1$ [*Rubinow and Keller*, 1961; *White and Schulz*, 1977; *Loth*, 2008], and thus overestimates the lift force caused by particle spin [*Hunt and Nalpanis*, 1985; *Shao*, 2000]. The particle angular velocity Ω_{p} is defined as positive for topspin (i.e., the particle rotates as if rolling in the same direction as it is moving), in which case the lift force is also positive (i.e., pointing upward). Experiments have shown that saltating particles predominantly have topspin, with Ω_{p} in the range of 100–1000 rev/s [*Chepil and Woodruff*, 1963; *White and Schulz*, 1977; *White*, 1982; *Xie et al.*, 2007; *Zou et al.*, 2007]. A likely reason for the predominance of topspin is that the shearing flow exerts a moment on the particles that produces topspin. Moreover, the friction on a particle's underside upon collision with the soil surface also produces torques that favor topspin over backspin. We assume that, after colliding with the surface, saltating particles have an initial spin of $\Omega_{\mathrm{p,0}} \approx 400 \pm 500$ rev/s, as suggested by experiments [*Chepil and Woodruff*, 1963; *White and Schulz*, 1977; *White*, 1982; *Xie et al.*, 2007; *Zou et al.*, 2007]. After leaving the surface, the particle spin is affected by the shear of the flow (which imparts topspin), and by viscous dissipation (which reduces the particle spin). Thus, after stochastically determining the particle's spin upon leaving the surface, we calculate the particle spin as a function of time by numerically integrating the differential equation [*Anderson and Hallet*, 1986; *Loth*, 2008]

$$\frac{d\Omega_{\mathrm{p}}}{dt} = \frac{60\mu}{\rho_{\mathrm{p}} D_{\mathrm{p}}^2}\left(\frac{1}{2}\frac{\partial U_{\mathrm{x}}}{\partial z} - \Omega_{\mathrm{p}}\right), \tag{6}$$

where the first term in the brackets on the right-hand side represents the moment exerted by the shearing flow and the second term denotes viscous dissipation. We neglect forces due to particle rotation that are not in the *xz* plane (see Figure 1) [*Xie et al.*, 2007].

2.1.2. Effect of Turbulence on Particle Trajectories

[18] Previous numerical models of saltation have often neglected the effects of turbulence on particle trajectories [e.g., *Anderson and Haff*, 1988; *McEwan and Willetts*,

1991], despite the fact that turbulence can substantially affect the trajectories of particles smaller than ~250 μm [*Anderson*, 1987]. We therefore do include the effects of turbulence on particles trajectories.

[19] The wind speed can be decomposed into the average wind speed and the turbulent fluctuation:

$$U_x = \overline{U_x} + U'_x;\ U_z = \overline{U_z} + U'_z \tag{7}$$

where $\overline{U}_x$, $\overline{U}_z$, U'_x, and U'_z are the time-averaged and turbulent horizontal and vertical components of the wind speed, respectively, at a given height. Although COMSALT is capable of simulating saltation on sloping terrain such as occurs on dunes [*Sauermann et al.*, 2001; *Huang et al.*, 2008], we assume horizontal flow (i.e., $\overline{U}_z = 0$) in the case studies presented in this article. The calculation of $\overline{U}_x$ in the near-surface layer where saltation takes place (the "saltation layer") is discussed in section 2.3. The turbulent fluctuation experienced by a fluid parcel moving with the flow can be described statistically by [*Van Dop et al.*, 1985; *Wilson and Sawford*, 1996]

$$U'_z(t+dt) - U'_z(t) = -\frac{U'_z(t)}{T_L}dt + n_G\sigma_w\sqrt{2dt/T_L}, \tag{8}$$

where a similar equation describes U'_x. Equation (8) has the discretized solution

$$U'_z(t+\Delta t) = U'_z(t)\exp(-\Delta t/T_L) + n_G\sigma_w\sqrt{2}\left[1-\exp\left(-\sqrt{\Delta t/T_L}\right)\right], \tag{9}$$

which in the limit $\Delta t \to dt$ reduces to equation (8). The model time step Δt is always set smaller than the Lagrangian timescale (T_L), and n_G is a Gaussian distributed random number with zero mean and unit standard deviation. For homogeneous, isotropic turbulence, the standard deviations of the horizontal and vertical turbulent wind speeds equal

$$\sigma_u = b_u\kappa z\left(\frac{\partial\overline{U_x}}{\partial z}\right);\ \sigma_w = b_w\kappa z\left(\frac{\partial\overline{U_x}}{\partial z}\right), \tag{10}$$

where $b_u = 1.4 \pm 0.1$ and $b_w = 2.5 \pm 0.1$ [*Hunt and Weber*, 1979; *Shao*, 1995; *Nishimura and Hunt*, 2000] and where $\kappa = 0.40$ is the von Kármán constant.

[20] The Lagrangian timescale T_L represents the approximate timescale over which the velocities experienced by a fluid parcel at times t and $t + T_L$ are statistically related. Since measurements are generally made in a stationary frame of reference, it is notoriously difficult to measure the Lagrangian timescale [*Leuning et al.*, 2000]. To the best of our knowledge, there have been no detailed studies of this timescale in saltation layers. However, the Lagrangian timescale of turbulent flow in forest and vegetation canopies has been studied in detail [*Raupach et al.*, 1996; *Leuning et al.*, 2000]. We thus use the analogy between turbulent flows in forest canopies and saltation layers [*Raupach*, 1991], and define T_L following equations (10) and (11) of *Leuning et al.* [2000] by equating the canopy height h_c to the height below which the bulk (i.e., 95%) of the saltation mass flux occurs.

[21] Equations (8)–(10) describe the turbulent fluctuations of the wind speed experienced by a particle moving along a flow streamline. However, gravitational forces and inertia cause the movement of saltating particles to deviate from that of fluid parcels [*Anderson*, 1987; *Sawford and Guest*, 1991]. The timescale T_L^* over which the fluctuations in wind speeds experienced by a saltating particle remain statistically correlated is thus shorter [*Csanady*, 1963], because a particle with nonzero velocity relative to the flow requires less time to traverse a turbulent eddy. Although these effects are still not fully understood [*Reynolds*, 2000], *Sawford and Guest* [1991] showed that a reasonable approximation for T_L^* for use with the fluctuation of the vertical flow speed is

$$T_L^* = T_L\left[1+(\beta v_R/\sigma_w)^2\right]^{-1/2}, \tag{11}$$

where $\beta = T_L/T_E$ is the ratio of the Lagrangian and Eulerian timescales, which is uncertain but is of order unity [*Sawford and Guest*, 1991; *Reynolds*, 2000; *Anfossi et al.*, 2006]. For horizontal velocity components (i.e., perpendicular to gravity),

$$T_L^* = T_L\left[1+(2\beta v_R/\sigma_u)^2\right]^{-1/2}. \tag{12}$$

To test the accuracy of equations (10)–(12), we used our model to simulate wind tunnel measurements of the dispersion of solid particles (see Figure 3) [*Snyder and Lumley*, 1971]. As in the work of *Sawford and Guest* [1991], we found poor agreement between our model and the results of experiments for the lightest particle (47 μm hollow glass), but found excellent agreement for the heavier particles (47 μm copper, 87 μm glass, and 87 μm corn pollen). Since the weight and relaxation time of particles that show good agreement are similar to those of saltating particles, we use the above parameterization in our model.

[22] We neglect the effect of saltating particles on the turbulence level (i.e., σ_u and σ_w), because measurements indicate that such effects are small [*Taniere et al.*, 1997; *Nishimura and Hunt*, 2000].

2.1.3. Full Equations of Motion

[23] We simulate the particle trajectories due to the gravitational and fluid forces described above. The full equations of motion are

$$ma_x = -\frac{\pi}{8}D_p^2\rho_a\left[C_d v_R(v_x-U_x) + D_p C_{L\Omega}^*\Omega_p(v_z-U_z) + \frac{12.92}{\pi}J^*\left(\frac{\mu}{\rho_a}\frac{\partial\overline{U_x}}{\partial z}\right)^{1/2}(v_z-U_z)\right] \tag{13a}$$

and

$$ma_z = -\frac{\pi}{8}D_p^2\rho_a\left[C_d v_R(v_z-U_z) + D_p C_{L\Omega}^*\Omega_p(v_x-U_x) + \frac{12.92}{\pi}J^*\left(\frac{\mu}{\rho_a}\frac{\partial\overline{U_x}}{\partial z}\right)^{1/2}(v_x-U_x)\right] - mg, \tag{13b}$$

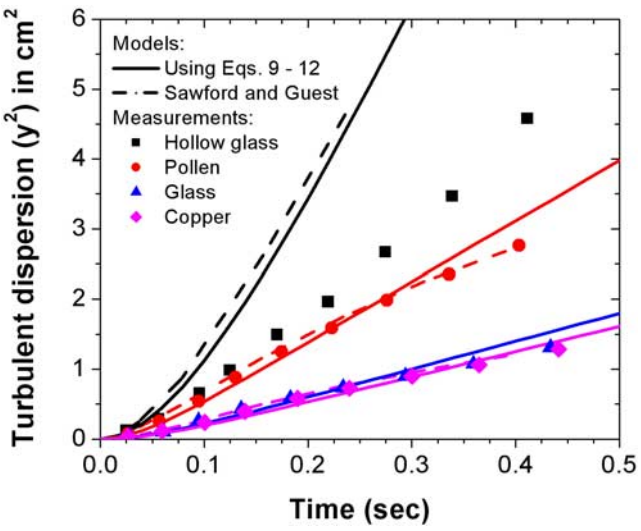

Figure 3. Turbulent dispersion perpendicular to the mean flow as measured by *Snyder and Lumley* [1971] for 46.5 μm diameter hollow glass (0.26 g/cm^3; black squares), 87.0 μm pollen (1.0 g/cm^3; red circles), 87.0 μm solid glass (2.5 g/cm^3; blue triangles), and 46.5 μm copper (8.9 g/cm^3; magenta diamonds) particles. Included for comparison are the turbulent dispersion simulated for similar particles by the model of *Sawford and Guest* [1991] (dashed black and colored lines) and by equations (9)–(12) (solid black and colored lines). Good agreement between model predictions and measurements can be seen, except for the hollow glass particles, which are the lightest of the four kinds of particles and are least characteristic of saltating particles.

where m is the particle's mass, v_x, v_z, a_x, and a_z are the particle speeds and accelerations in the x and z directions, respectively, and g = 9.8 m/s^2 is the gravitational acceleration. The first term on the right-hand side accounts for fluid drag, the second accounts for particle spin, and the third accounts for the Saffman force. The model uses the fourth-order Adams-Moulton method [*Hairer et al.*, 1993] to numerically integrate the equations of motion and obtain the particle trajectories. In order to lower the computational cost, COMSALT explicitly calculates the trajectories of only a fraction of the total number of saltating particles and considers those trajectories to represent the entire ensemble of particle trajectories. Sensitivity studies showed that increasing the number of explicitly simulated particle trajectories beyond the number used to obtain the results presented in this article does not substantially affect the model results.

2.1.4. Sensitivity of Particle Trajectories to Fluid Lift Forces and Turbulence

[24] One of the improvements of COMSALT over most previous models is that it includes the effects of the Magnus and Saffman lift forces [*Rubinow and Keller*, 1961; *Saffman*, 1965, 1968; *White and Schulz*, 1977; *Loth*, 2008] as well that of fluid turbulence on the particle trajectories. In Figure 4, we test the sensitivity of particle trajectories to these three separate effects.

[25] We find that the Saffman force due to the shearing flow is many orders of magnitude smaller than the gravitational and fluid drag forces. The Saffman force can therefore be safely neglected without noticeably affecting particle trajectories. On the other hand, the Magnus lift force due to particle rotation has typical values of a few percent of the particle's weight and therefore does substantially affect particle trajectories, as also indicated by laboratory studies [*White and Schulz*, 1977; *White*, 1982; *Zou et al.*, 2007]. Finally, we find that fluid turbulence substantially affects the trajectories of smaller saltating particles. The effect of turbulence on larger saltating particles is much less pronounced, because of the larger inertia and thus smaller susceptibility to fluid velocity perturbations of these particles. Note that the effect of turbulence on particle trajectories increases with shear velocity and can thus become important also for larger particles at large shear velocities.

2.2. Particle Collisions With the Surface

[26] The collision of saltating particles with the surface (Figure 1) is a key physical process in saltation, as it splashes new saltating particles into the fluid stream [*Anderson and Haff*, 1991; *Shao*, 2000]. Moreover, the collision of saltating particles with the soil converts horizontal momentum into vertical momentum, since particles strike the soil nearly horizontally, and rebound at angles of $\sim$15–70° from horizontal [*Anderson and Haff*, 1988, 1991; *Willetts and Rice*, 1985, 1986, 1989; *Nalpanis et al.*, 1993; *Rice et al.*, 1995]. This conversion of horizontal momentum into vertical momentum is essential, as it allows saltating particles to replenish the vertical momentum that is dissipated through fluid drag.

2.2.1. Rebounding Particle

[27] While particle trajectories can be calculated based on simple physical principles (see section 2.1), the collision of saltating particles with the soil surface is inherently a stochastic process. For example, not all saltating particles rebound from the surface, even when they impact it at high speed [*Mitha et al.*, 1986; *Anderson and Haff*, 1991]. The probability that a saltating particle will rebound upon impact can be approximated by [*Anderson and Haff*, 1991]

$$P_{\mathrm{reb}} = B\left\lfloor 1 - \exp\left(-\gamma v_{\mathrm{imp}}\right)\right\rfloor, \tag{14}$$

where v_{imp} is the speed with which the particle impacts the surface. *Mitha et al.* [1986] determined the parameter B to be 0.94 for 4 mm steel particles, while the two-dimensional numerical simulations of *Anderson and Haff* [1991] found a similar value of $B \approx 0.95$ for 230 and 320 μm sand particles. To the best of our knowledge, the parameter γ has not been experimentally determined, but the numerical simulations of *Anderson and Haff* [1988, 1991] indicate that it is of order 2 s/m.

[28] We use results of laboratory and numerical studies to describe the velocity of rebounding particles [*White and Schulz*, 1977; *Mitha et al.*, 1986; *Anderson and Haff*, 1991; *McEwan and Willetts*, 1991; *Nalpanis et al.*, 1993; *Rice et al.*, 1995; *Rioual et al.*, 2000; *Oger et al.*, 2005; *Beladjine et al.*, 2007; *Kang et al.*, 2008]. Recent laboratory experiments have shown that the fraction of kinetic energy retained by the rebounding particle is approximately normally distributed [*Wang et al.*, 2008] while the rebounding angle approximately follows an exponential distribution [*Willetts and Rice*, 1985, 1986; *McEwan and Willetts*, 1991; *Rice et*

al., 1996; *Kang et al.*, 2008]. We thus take the kinetic energy of the rebounding particles to be 45 ± 22% of the impacting kinetic energy, and the rebound angle as an exponential distribution with a mean of 40° from horizontal.

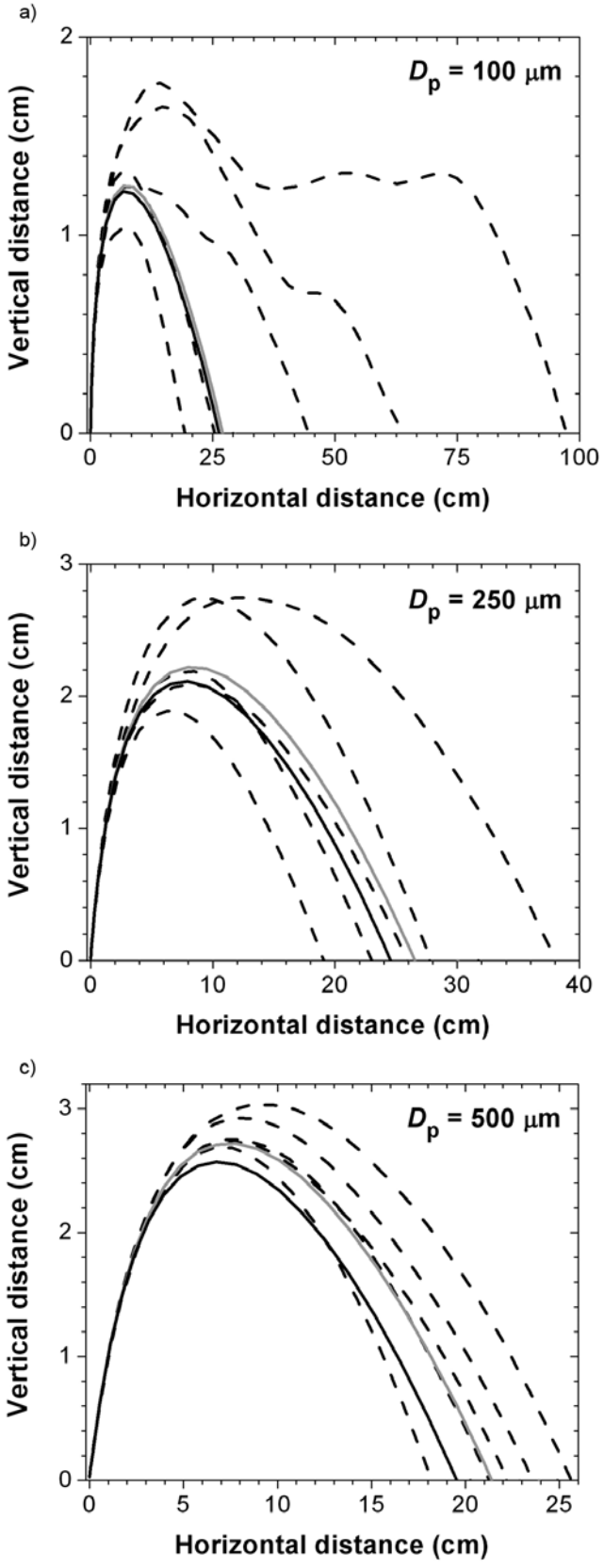

Figure 4. Sensitivity study of trajectories of saltating particles with diameters of (a) 100, (b) 250, and (c) 500 μm that are launched from the surface with a speed of 1 m/s and an angle of 40° from horizontal. The vertical wind speed profile and turbulence characteristics were obtained by running COMSALT at u^* = 0.4 m/s for the size distribution reported by *Namikas* [2003]. The solid lines denote trajectories that do not include the effects of turbulence and the Magnus force, gray lines do include the effects of the Magnus force with an assumed particle spin of 400 rev/s, and dashed lines denote five (stochastic) particle trajectory simulations including both the effects of turbulence and the Magnus force. Including the Saffman force does not noticeably alter the particle trajectories, since the Saffman force is many orders of magnitude smaller than the gravitational and fluid forces.

2.2.2. Ejection Speed of Splashed Surface Particles

[29] In steady state saltation, the loss of particles through the process represented by equation (14) is balanced by the splashing of surface particles. The "splash function," which describes the number and velocity of the ejected surface particles as a function of the velocity of the impacting particle [*Ungar and Haff*, 1987], is thus a key component of numerical models of saltation [*Werner*, 1990; *Anderson and Haff*, 1988, 1991; *McEwan and Willetts*, 1991, 1993; *Shao and Li*, 1999]. Instead of using an empirical expression for the splash function that is based on the results of laboratory or numerical experiments, as most previous models have done, we derive a physically based expression of the splash function below.

[30] The ejection of particles from the surface by impacting saltating particles is constrained by the conservation of both energy and momentum. These constraints can be expressed as

$$\varepsilon_{\mathrm{reb}} + \varepsilon_{\mathrm{ej}} + \varepsilon_{\mathrm{F}} = 1 \tag{15a}$$

and

$$\alpha_{\mathrm{reb}} + \alpha_{\mathrm{ej}} + \alpha_{\mathrm{F}} = 1, \tag{15b}$$

where ε and α refer to the partitioning of energy and momentum, respectively, and the subscripts refer to the fraction of the total energy or momentum contained in the rebounding particle (reb), the ejected particles (ej), and that lost through frictional processes (F). In order to derive a physically based expression of the number and speed of ejected particles, we need to determine whether energy conservation or momentum conservation is the dominant constraint on the ejection of surface particles. To determine this, we unrealistically neglect friction (i.e., $\varepsilon_{\mathrm{F}} = \alpha_{\mathrm{F}} = 0$) in the collision of a particle of mass m_{imp} with a bed of particles with mass m_{ej}, such that we can obtain the maximum number of particles that can be ejected without violating conservation of energy (N^E_{max}) or momentum (N^M_{max}). This yields

$$N^E_{\mathrm{max}} = \frac{(1-\varepsilon_{\mathrm{reb}}) m_{\mathrm{imp}} v^2_{\mathrm{imp}}}{m_{\mathrm{ej}} \left\langle v^2_{\mathrm{ej}} \right\rangle + 2\phi} \tag{16a}$$

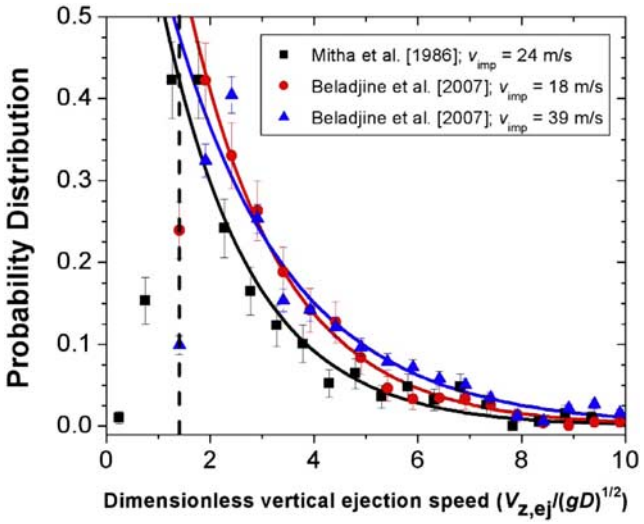

Figure 5. Probability distribution of the dimensionless vertical ejection speed. Shown are experimental results for 4 mm steel particles impacting a bed of similar particles at 24 m/s (black squares) [*Mitha et al.*, 1986] and for 6 mm PVC particles impacting at 18 m/s (red circles) and 39 m/s (blue triangles) [*Beladjine et al.*, 2007]. The data above the threshold for which particle detection is reliable (dashed line) [*Beladjine et al.*, 2007] are well-described by exponential distributions (black, red, and blue solid lines). Error bars are derived from the total number of particle counts contained in each data point.

and

$$N_{\max}^{M} = \frac{(1-\alpha_{\mathrm{reb}})m_{\mathrm{imp}}v_{\mathrm{imp}}}{m_{\mathrm{ej}}\langle v_{\mathrm{ej}}\rangle}, \tag{16b}$$

where φ is the energy with which soil particles are bonded with each other, $\langle v_{\mathrm{ej}}\rangle$ is the ensemble-averaged ejected particle speed (that is, the speed of ejected particles averaged over many impacts on the soil surface of a particle with a given speed), and $\langle v_{\mathrm{ej}}^2\rangle$ is the ensemble-averaged square of the ejected particle speed.

[31] In order to compare $N_{\max}^{E}$ and $N_{\max}^{M}$ we need to relate $\langle v_{\mathrm{ej}}^2\rangle$ to $\langle v_{\mathrm{ej}}\rangle$. We obtain such a relation by assuming a functional form for the probability distribution $P(v_{\mathrm{ej}})$ of the speed of ejected particles. The numerical simulations of *Anderson and Haff* [1991] found that $P(v_{\mathrm{ej}})$ takes the form of an exponential distribution, which is also suggested by experimental results (see Figure 5). We thus take [*Werner*, 1990; *Sorensen*, 1991; *Anderson and Haff*, 1991]

$$P(v_{\mathrm{ej}}) = \frac{\exp\left(-v_{\mathrm{ej}}/\langle v_{\mathrm{ej}}\rangle\right)}{\langle v_{\mathrm{ej}}\rangle}. \tag{17}$$

We find from equation (17) that $\langle v_{\mathrm{ej}}^2\rangle = 2\langle v_{\mathrm{ej}}\rangle^2$, which we combine with equations (16a) and (16b) to obtain the critical impact speed v_{imp}^{crit} at which the constraints posed by energy and momentum conservation are equally restricting (i.e., where $N_{\max}^{E} = N_{\max}^{M}$). This yields

$$v_{\mathrm{imp}}^{crit} = \frac{2}{1+\alpha_{\mathrm{reb}}}\left[\langle v_{\mathrm{ej}}\rangle + \phi/m_{\mathrm{ej}}\langle v_{\mathrm{ej}}\rangle\right] \approx \frac{2\langle v_{\mathrm{ej}}\rangle}{1+\alpha_{\mathrm{reb}}}, \tag{18}$$

where we used that $\varepsilon_{\mathrm{reb}} = \alpha_{\mathrm{reb}}^2$ and assumed that $\phi \ll m_{\mathrm{ej}}\langle v_{\mathrm{ej}}\rangle^2$ for loose sand, as is typical for saltation on dry dunes and beaches. When $v_{\mathrm{imp}} \ll v_{\mathrm{imp}}^{crit}$, we have that $N_{\max}^{E} \ll N_{\max}^{M}$, such that energy conservation constrains the number of surface particles that can be ejected. Conversely, when $v_{\mathrm{imp}} \gg v_{\mathrm{imp}}^{crit}$, we find that $N_{\max}^{E} \gg N_{\max}^{M}$, such that momentum conservation becomes the main constraint. Since the speed of ejected particles is approximately an order of magnitude smaller than the impacting speed [e.g., *Rice et al.*, 1995], we find that generally $v_{\mathrm{imp}} \gg v_{\mathrm{imp}}^{crit}$ and thus that $N_{\max}^{E} \gg N_{\max}^{M}$. This implies that the splashing of loose sand particles from the surface by saltating particles is limited primarily by momentum conservation and not as much by energy conservation. While the inclusion of frictional processes will affect the exact value of v_{imp}^{crit}, it is unlikely to alter this general conclusion. Note however that the ejection of dust particles from the soil is rather different because in this case φ is not small. Therefore energy conservation might be the dominant constraint limiting the number of ejected dust particles. Indeed, this is what measurements by *Shao et al.* [1993] suggest.

[32] We thus impose conservation of momentum on the number of surface particles that can be ejected and thereby find that

$$N(v_{\mathrm{imp}})m_{\mathrm{ej}}\langle v_{\mathrm{ej}}\rangle = \langle \alpha_{\mathrm{ej}}\rangle m_{\mathrm{imp}}v_{\mathrm{imp}}, \tag{19}$$

where $\langle \alpha_{\mathrm{ej}}\rangle$ is the ensemble-averaged fraction of the impacting momentum that is spent on splashing particles from the surface and N is the average number of ejected particles, which depends on the particle impact speed v_{imp}. We neglect the dependence of N on the impact angle [*Beladjine et al.*, 2007] because the range of angles with which saltating particles impact the surface is relatively narrow [e.g., *Wang et al.*, 2008]. Both laboratory and modeling studies suggest that the number of ejected particles scales approximately linearly with the impact speed [*Anderson and Haff*, 1988, 1991; *McEwan and Willetts*, 1991; *Rice et al.*, 1996; *Rioual et al.*, 2000; *Oger et al.*, 2005; *Beladjine et al.*, 2007],

$$N \approx Av_{\mathrm{imp}}. \tag{20}$$

Dimensional analysis [*Andreotti*, 2004; *Beladjine et al.*, 2007] and conservation of momentum suggests that the parameter A can be rewritten as

$$A = \frac{a}{\sqrt{gD}}\frac{m_{\mathrm{imp}}}{m_{\mathrm{ej}}}, \tag{21}$$

where D is a typical particle size ($\sim$250 μm for saltation on Earth) and a is a dimensionless constant that is independent of the impacting velocity and the masses of the impacting and ejected particles and lies in the range of 0.01–0.05 [*Willetts and Rice*, 1985, 1986, 1989; *McEwan and Willetts*,

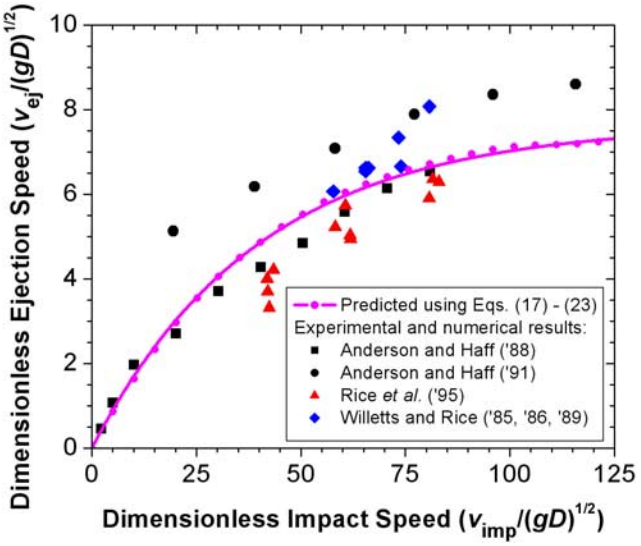

Figure 6. The average dimensionless speed of ejected surface particles ($\overline{v_{ej}}/\sqrt{gD}$) as a function of the dimensionless speed of the impacting particle ($\overline{v_{imp}}/\sqrt{gD}$). We used equations (17)–(23) to perform a Monte Carlo simulation (magenta circles) of particles impacting a bed of similar particles, for which we used parameters as specified in Table 1. The model results do not depend on the particle size. The magenta solid line represents the fit to these results as given by equation (24). Experimental results from *Willetts and Rice* [1985, 1986, 1989] (red triangles) denote the average speed of particles splashed from a bed of mixed particles by a medium-sized (250–355 μm) impacting particle, whereas the results from *Rice et al.* [1995] (blue diamonds) represent the average speed by which fine (150–250 μm), medium (250–355 μm), and coarse (355–600 μm) particles are ejected from a bed of mixed particles by an impacting particle of the same size. The numerical studies of *Anderson and Haff* [1988, 1991] (black squares and circles, respectively) were performed for two-dimensional sand grains of 1 mm and 230–320 μm diameter, respectively. Results from similar experimental and numerical studies with particles other than sand grains [e.g., *Oger et al.*, 2005; *Beladjine et al.*, 2007] are omitted. The sphericity and the elastic and friction coefficients of such particles differ from those of natural sand, which likely affects the experimental results [*Mitha et al.*, 1986; *Anderson and Haff*, 1991].

1991; *Rice et al.*, 1995, 1996]. Combining equations (19)–(21) then yields the simple expression

$$\langle v_{ej} \rangle = \frac{\langle \alpha_{ej} \rangle \sqrt{gD}}{a}. \tag{22}$$

Thus, assuming that the fraction of momentum spent on splashing particles from the surface ($\langle \alpha_{ej} \rangle$) does not depend on impact speed [*Andreotti*, 2004], the average speed of ejected particles should be independent of the impact speed. This is indeed consistent with results for large impact speeds from laboratory experiments; *Werner* [1987, 1990] found that $\langle v_{ej} \rangle$ remains approximately constant for a dimensionless impact speed larger than ~68 and *Rioual et al.* [2000] and *Beladjine et al.* [2007] reported similar results.

[33] Equation (22) is however only valid for large impact speeds, where $N \gg 1$, such that momentum and energy conservation are automatically satisfied by the statistical (ensemble) approach of equations (17) and (19). For smaller impact speeds, for which $N \approx 1$, the speed of ejected particles can no longer be approximated by equation (22) because momentum and energy conservation do not allow the high-speed tail of the exponential distribution of impact speeds of equation (17) with $\langle v_{ej} \rangle$ defined by equation (22). Thus, for smaller impact speeds, the discrete nature of the ejection process (that is, $N \approx 1$ rather than $N \gg 1$) provides explicit constraints on momentum and energy conservation that are not automatically satisfied by equations (17) and (19),

$$\sum_i m_{ej}^i v_{ej}^i \le (1 - \alpha_{reb}) m_{imp} v_{imp} \tag{23a}$$

and

$$\sum_i m_{ej}^i v_{ej}^{i^2} \le (1 - \alpha_{reb}^2) m_{imp} v_{imp}^2, \tag{23b}$$

where the superscript i sums over all the ejected particles and where we again used that $\varepsilon_{reb} = \alpha_{reb}^2$. When the impacting particle has only enough energy to at most eject one surface particle, equations (23a) and (23b) thus truncate the probability distribution of ejection speeds given by equation (17). This leads to a decrease in the average ejected particle speed for small impact speeds, as was indeed found by numerical [*Anderson and Haff*, 1988, 1991] and experimental studies with natural sand [*Willetts and Rice*, 1985, 1986, 1989; *Rice et al.*, 1995]. Note that the constraints of energy and momentum conservation described by equations (23) are automatically satisfied in equations (17) and (19) when $N \gg 1$.

[34] Figure 6 compares $\langle v_{ej} \rangle$ obtained from a Monte Carlo simulation using equations (17), (20), (21), (23) with results from experimental [*Willetts and Rice*, 1985, 1986, 1989; *Rice et al.*, 1995] and numerical [*Anderson and Haff*, 1988, 1991] studies. The increase of $\langle v_{ej} \rangle$ at low v_{imp} is reproduced by our analytical model, as is the independence of $\langle v_{ej} \rangle$ for larger v_{imp} reported in the literature [*Werner*, 1987, 1990; *Haff and Anderson*, 1993; Rioual et al. 2000; *Oger et al.*, 2005; *Beladjine et al.*, 2007]. These two physical limits can now be interpreted: for low dimensionless impact speed ($N \approx 1$) the increase in ejected particle momentum with increasing impact speed is spent on the single ejected particle, thus producing the increase in $\langle v_{ej} \rangle$ seen in Figure 6. But for large dimensionless impact speed ($N \gg 1$) the increase in ejected particle momentum with increasing impact speed is spent on ejecting more particles. Indeed, since the number of splashed particles is proportional to the impacting momentum, it follows that, for large impact speeds, $\langle v_{ej} \rangle$ must remain constant with impact speed to satisfy momentum conservation.

[35] The average dimensionless ejection speed presented in Figure 6 can be described by the expression

$$\frac{\langle v_{ej}\rangle}{\sqrt{gD}} = \frac{\langle \alpha_{ej}\rangle}{a}\left[1 - \exp\left(-\frac{v_{imp}}{40\sqrt{gD}}\right)\right], \quad (24)$$

such that equation (22) is retrieved for very large dimensionless impact speeds, where $N \gg 1$. Equation (24) thus constitutes a physically based expression of the speed of ejected particles, which shows good agreement with experiments (Figure 6). The distribution of ejection speeds for the whole range of N is well-described by the exponential distribution of equation 17, with $\langle v_{ej}\rangle$ given by equation 24.

2.2.3. Ejection Angle of Splashed Surface Particles

[36] Since the collision of soil particles with the surface converts horizontal momentum into vertical momentum, there are no convenient energetic constraints on the angles at which particles are ejected. We therefore use the consensus result of laboratory and numerical studies that the angle at which particles are ejected can be described by an exponential distribution with a mean of 50° from horizontal [*Willetts and Rice*, 1985, 1986, 1989; *Anderson and Haff*, 1988, 1991; *Werner*, 1990; *McEwan and Willetts*, 1991; *Rice et al.*, 1995, 1996].

2.2.4. Ejection of Particles From Mixed Soils

[37] The above analysis of the splash function can be easily extended to mixed soils by assuming that a particle's chance of being ejected from the surface depends on its cross-sectional area [*Rice et al.*, 1995; *Shao and Mikami*, 2005]. For a mixed soil, the number of particles ejected from each particle size bin then becomes

$$N^k = \frac{a}{\sqrt{gD}}\frac{m_{imp}}{m_{ej}^k}\left(\frac{D_{ej}^k}{D_{imp}}\right)^2 v_{imp} f^k = \frac{a}{\sqrt{gD}}\frac{D_{imp}}{D_{ej}^k} v_{imp} f^k, \quad (25)$$

where D_{imp} and D_{ej}^k are the diameter of the impacting and ejected particles and f^k denotes the mass fraction of the kth particle bin of the soil's particle size distribution.

2.3. Wind Profile

[38] In addition to the particle trajectories (section 2.1) and the collision of saltating particles with the surface (section 2.2), the modification of the wind profile through momentum transfer to saltating particles is a key process in saltation. The wind profile over an aerodynamically rough surface in the absence of momentum transfer to saltating particles [*Prandtl*, 1935; *Bagnold*, 1941] is given by

$$\overline{U_x}(z) = \frac{u^*}{\kappa}\ln\left(\frac{z}{z_0}\right), \quad (26)$$

where z is the vertical distance from the surface, u^* is the wind shear velocity or friction velocity and is a measure of the gradient of the fluid flow field, and $z_0 \approx D/30$ is the surface roughness [*Nikuradse*, 1933], where D is the characteristic size of soil particles.

[39] The initial wind profile given by (26) is modified by the transfer of momentum between the wind flow and saltating particles. The amount of horizontal fluid momentum that fluxes into the saltation layer depends directly on the shearing of the flow and is equal to the fluid shear stress $\tau = \rho_a u^{*2}$ above the saltation layer. At steady state, this flux of horizontal momentum into the saltation layer is partitioned between saltating particles (τ_p) and the fluid (τ_a), such that [*Raupach*, 1991]

$$\tau = \tau_a(z) + \tau_p(z). \quad (27)$$

The fluid momentum flux $\tau_a(z)$ in the saltation layer is a function of the velocity gradient,

$$\tau_a(z) = \rho_a\left[\kappa z\frac{\partial \overline{U_x}(z)}{\partial z}\right]^2, \quad (28)$$

and $\tau_a(z) = \tau$ for z above the saltation layer. Combining equations (27) and (28) then yields

$$\frac{\partial \overline{U_x}(z)}{\partial z} = \frac{1}{\kappa z}\sqrt{u^{*2} - \tau_p(z)/\rho_a}, \quad (29)$$

with the particle momentum flux given by [*Shao*, 2000]

$$\tau_p(z) = \sum_i m^i v_x^i(z) - \sum_j m^j v_x^j(z), \quad (30)$$

where the superscripts i and j sum over all descending and ascending particles, respectively, that pass the height z per unit area and unit time.

[40] We calculate $\tau_p(z)$ as a function of the particle trajectories (see section 2.1) and the concentration of saltating particles (see below), and use it to numerically integrate equation (29) to obtain the wind profile in the saltation layer. Note that COMSALT follows previous investigators [e.g., *Anderson and Haff*, 1988, 1991; *Shao and Li*, 1999; *Almeida et al.*, 2006] and for simplicity assumes that the soil surface is flat. We thus neglect the effect of sand ripples with typical heights of several mm, which usually form during saltation on dunes and beaches [*Bagnold*, 1941].

2.4. Particle Concentration

[41] The concentration of saltating particles is affected by both the capture of impacting saltating particles by the soil bed (equation (14)) and the production of new saltating particles through splashing (equation (25)). The concentration n^k of saltating particles in the particle bin k is thus described by

$$\frac{dn^k}{dt} = \sum_i \frac{a}{\sqrt{gD}}\frac{D_{imp}^i}{D_{ej}^k} v_{imp}^i f^k - \sum_{j_k} 1 - B\left[1 - \exp\left(-\gamma v_{imp}^{j_k}\right)\right], \quad (31)$$

where i and j_k respectively sum over all saltating particles and over all particles in bin k that are impacting the soil surface per unit time and unit area. The first term on the right-hand side accounts for the production of saltating particles through splashing and the second term accounts for the loss of saltating particles to the soil. As the model progresses through successive iterations (see Figure 2), it

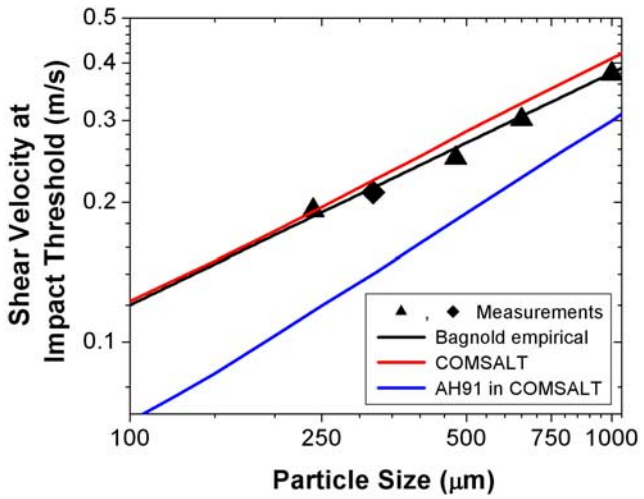

Figure 7. Impact threshold for Earth ambient conditions as measured in wind tunnel experiments by *Bagnold* [1937] (triangles) and *Iversen and Rasmussen* [1994] (diamond), and predicted by COMSALT with the splash function described in section 2.2 (red line) and with the splash function described in section 8 of *Anderson and Haff* [1991] (blue line). Also plotted is Bagnold's empirical relation for the impact threshold (black line) [*Bagnold*, 1937, p. 435].

uses equation (31) to converge to the steady state particle concentration. Indeed, if the number of splashed surface particles is greater than the number of saltating particles settling back to the soil surface, then the concentration of saltating particles increases. This augments the particle momentum flux and thus decreases the wind speed (equation (29)), which lowers the typical impact speed of saltating particles, thus reducing the number of splashed particles. If, on the other hand, the number of splashed particles is insufficient to balance the settling of saltating particles back to the soil surface, then the particle concentration will decrease. This increases the wind speed and thus the typical impact speed, which in turn increases the number of splashed particles. The model thus iteratively adjusts the particle concentration until steady state is reached and the particle concentration remains constant with time (i.e., $dn^k/dt = 0$, for all k). In steady state, we then have that

$$\sum_i \frac{a}{\sqrt{gD}} \frac{D^i_{\mathrm{imp}}}{D^k_{\mathrm{ej}}} v^i_{\mathrm{imp}} f^k = \sum_{j_k} 1 - B\left[1 - \exp\left(-\gamma v^{j_k}_{\mathrm{imp}}\right)\right], \quad (32)$$

for all k. As mentioned in section 1, the stochastic nature of the interaction of saltating particles with the soil surface and with the turbulent wind field means that the model reaches a dynamic balance in which equation (32) is satisfied over longer timescales (a few seconds [*Anderson and Haff*, 1988, 1991; *Jackson and McCloskey*, 1997]). We believe this is an accurate representation of natural saltation.

[42] Since the parameters a, B, and γ in equations (31) and (32) have not been precisely determined by measurements (Table 1), a useful constraint on their values is that equation (32) must be satisfied at the impact threshold. Since the particle concentration (and thus $\tau_p(z)$ in equation (29)) is small at the impact threshold, the wind profile is simply given by equation (26), such that particle trajectories are obtained in a straightforward manner. Indeed, for given values of the parameters a, B, and γ, we can calculate the value of the impact threshold at which equation (32) is satisfied. We find that the functional form of the impact threshold is reproduced almost independently of the values of these parameters and that $a = 0.020$, $B = 0.96$, and $\gamma = 1.0$ s/m provides good quantitative agreement with measurements of the impact threshold (see Figure 7). These parameter values are in agreement with available laboratory and numerical experiments (Table 1). To our knowledge, no previous numerical models of saltation have been able to reproduce measurements of the impact threshold and the good agreement in Figure 7 thus supports the correctness of our splash parameterization. Indeed, when we implement the influential splash function of *Anderson and Haff* [1991] (see their section 8; note the typo in their equation (10)) instead of the parameterization outlined in section 2.2, the agreement is not nearly as good. The main reason for this difference is probably an overestimation of the number of ejected grains in the Anderson and Haff splash function, when compared with experiments [*Anderson and Haff*, 1991].

[43] An additional constraint on the values of a, B, and γ can be obtained by using equation (32) to determine an approximate average impact speed in steady state saltation. This can be done by assuming that particle impact speeds are exponentially distributed (see equation (17)), as previous studies have suggested [*Anderson and Hallet*, 1986] and results from our model indicate (J. F. Kok, manuscript in preparation, 2009). Solving equation (32) for the average impact speed in this manner yields $\overline{v_{\mathrm{imp}}} \approx 1.2$ m/s for 250 μm particles. Note that assuming different plausible impact speed distributions, such as a gamma function [*White and Schulz*, 1977], yields only slightly different values of $\overline{v_{\mathrm{imp}}}$. Since the average impact speed is independent of shear velocity [*Ungar and Haff*, 1987; *Andreotti*, 2004], as also found by our model simulations (Kok, manuscript in preparation, 2009), we expect particle speeds for different shear velocities to converge near the surface. Recent measurements of particle speeds using several particle imagining techniques in a wind tunnel [*Rasmussen and Sorensen*, 2008; *Creyssels et al.*, 2009] have indeed found that particle speeds for different shear velocities converge to a common value of $\sim$1.0–1.5 m/s at the surface. This agreement between measurements and the qualitative and quantitative predictions of our model further supports the physical basis underlying our splash parameterization and the chosen values for the parameters a, B, and γ.

3. Testing of the Model With Measurements

[44] We test our model by comparing its results to measurements of the horizontal and vertical profiles of particle mass flux, the total height-integrated mass flux, the size distribution of saltating particles, and the wind profile and aerodynamic roughness length during saltation. When available, we use field measurements rather than wind tunnel measurements since recent studies have shown

Table 1. Description of Parameters Used in the Numerical Model[a]

Variable	Physical Meaning	Relevant Literature	Range in Literature	Value Used in Model	Relative Uncertainty	Relative Sensitivity
$\langle\alpha_{ej}\rangle$	Average fraction of impacting momentum spent on ejecting surface grains	*Rice et al.* [1995]	0.14–0.20	$\frac{\langle 1-\sqrt{\varepsilon_{reb}}\rangle}{2.5} \approx 0.15$	Medium	Medium
β	The ratio of the Lagrangian and Eulerian time scales	*Anfossi et al.* [2006]	0.3–4	1	High	Low
$\langle\varepsilon_{reb}\rangle$	Average fraction of impacting kinetic energy retained by rebounding particle	*Wang et al.* [2008]	0.43–0.46	0.45	Medium	High
γ	Parameter that scales the exponential decay with impact speed of a saltating particle's rebound probability	*Anderson and Haff* [1991]	~2	1	Very high	Low
θ_{ej}	The mean of the exponential distribution that describes the angle from horizontal with which a surface particle is ejected	*Willetts and Rice* [1985, 1986, 1989]; *Anderson and Haff* [1988, 1991]; *McEwan and Willetts* [1991]; *Rice et al.* [1995, 1996]	40°–60°	50°	Low	Low
θ_{reb}	The mean of the exponential distribution that describes the angle from horizontal with which a saltating particle rebounds	*White and Schulz* [1977]; *Willetts and Rice* [1985, 1986, 1989]; *Anderson and Haff* [1988, 1991]; *McEwan and Willetts* [1991]; *Nalpanis et al.* [1993]; *Rice et al.* [1995, 1996]; *Kang et al.* [2008]	25°–50°	40°	Low	Medium
ρ_a (kg/m^3)	Air density – calculated using the ideal gas law with P = 101325 Pa, T = 300 K, and a molar mass of 28.9 g	NA	NA	1.174	NA	NA
ρ_p (g/cm^3)	Particle density	NA	NA	2.65	Very low	Low
$\sigma_{\varepsilon_{reb}}$	Standard deviation of the normal distribution that describes the fraction of kinetic energy that is retained upon rebound	*Wang et al.* [2008]	0.17–0.22	0.22	High	Low
σ_{Ω_p} (rev/s)	Standard deviation of the normal distribution that describes the particle spin upon leaving the surface of rebounding or ejected grains	*Chepil and Woodruff* [1963]; *White and Schulz* [1977]; *White* [1982]; *Xie et al.* [2007]; *Zou et al.* [2007]	Unclear	500	Very high	Very low
Ω_p (rev/s)	Mean of the normal distribution that describes the particle spin upon leaving the surface of rebounding and ejected grains	*Chepil and Woodruff* [1963]; *White and Schulz* [1977]; *White* [1982]; *Xie et al.* [2007]; *Zou et al.* [2007]	100–1000	400	High	Low
a	Dimensionless constant that scales proportionality between impact speed and number of ejected particles	*McEwan and Willetts* [1991]; *Rice et al.* [1995, 1996]	0.01–0.05	0.02	Medium	High
b_u (m/s)	The standard deviation of the turbulent horizontal wind speed	*Shao* [1995]; *Nishimura and Hunt* [2000]	2.4–2.5	2.5	Low	Very low
b_w (m/s)	The standard deviation of the turbulent vertical wind speed	*Hunt and Weber* [1979]; *Shao* [1995]; *Nishimura and Hunt* [2000]	1.2–1.5	1.4	Low	Low
B (s/m)	Probability that a high-speed particle rebounds upon impacting the soil surface	*Mitha et al.* [1986]; *Anderson and Haff* [1991]	~0.94–0.95	0.96	High	Medium

[a]NA means not applicable.

wind tunnel measurements to differ significantly and systematically from measurements of natural saltation [*Farrell and Sherman*, 2006; *Sherman and Farrell*, 2008].

[45] The values of the model parameters used for the results presented in this article are listed in Table 1. We have also included a subjective estimate of the uncertainty of these parameters, as well as a relative indication of the model sensitivity. We hope these estimates can help guide future experimental studies of saltation.

3.1. Particle Mass Flux Profiles

[46] Detailed field measurements of the variation of the particle mass flux with height were made by several investigators and are summarized by *Farrell and Sherman* [2006]. Our model shows good agreement with such vertical mass flux profiles as measured by *Greeley et al.* [1996] and *Namikas* [2003] for low (u^* = 0.31 m/s) and medium (u^* = 0.48 m/s) shear velocities (Figures 8a and 8b). For larger shear velocities (u^* = 0.63 m/s), our model under-

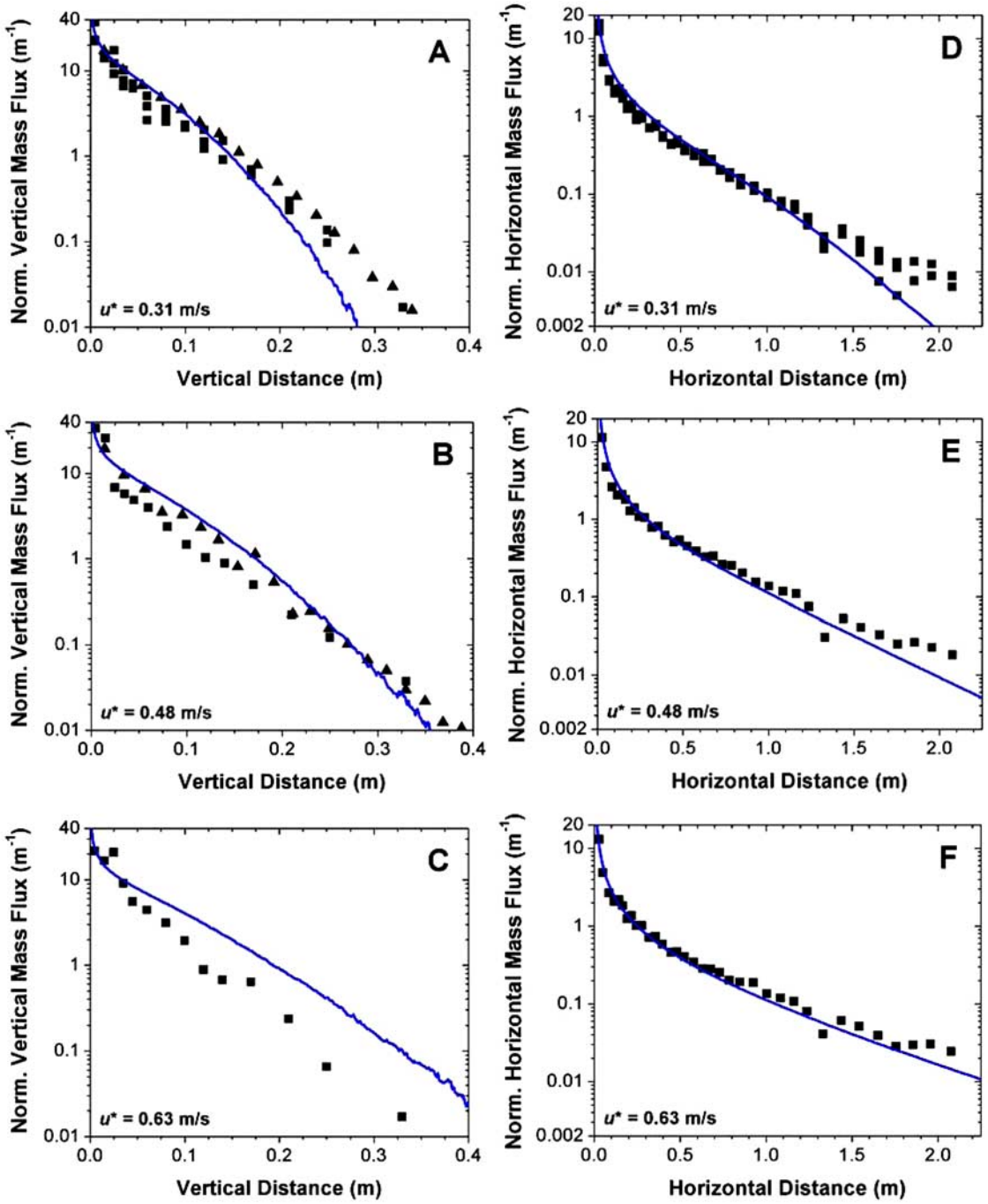

Figure 8. Vertical and horizontal mass flux profiles for u^* = 0.31, 0.48, and 0.63 m/s. Triangles denote vertical mass flux profile measurements from runs 4 and 5b of *Greeley et al.* [1996] and squares denote both vertical and horizontal mass flux profile measurements from runs 4, 5, 8, 13, and 14 of *Namikas* [2003]. Model results (solid blue line) were obtained for the size distribution reported in *Namikas* [2003], which we assume characteristic for Greeley et al.'s measurements as well, since their measurements were taken at a similar location. Both measured and modeled mass flux profiles were normalized by their total mass flux to facilitate comparison.

estimates the decrease in horizontal mass flux with height (Figure 8c). A possible reason for this is the absence in the present model version of electrostatic forces, which are thought to decrease the height of particle trajectories as the wind speed increases [*Kok and Renno*, 2008]. Detailed measurements of the horizontal profile of the particle mass flux (i.e., the variation of the particle deposition rate with horizontal distance from a certain starting point) have also been made by *Namikas* [2003]. Simulations with our model show excellent agreement with these measurements (Figures 8d–8f).

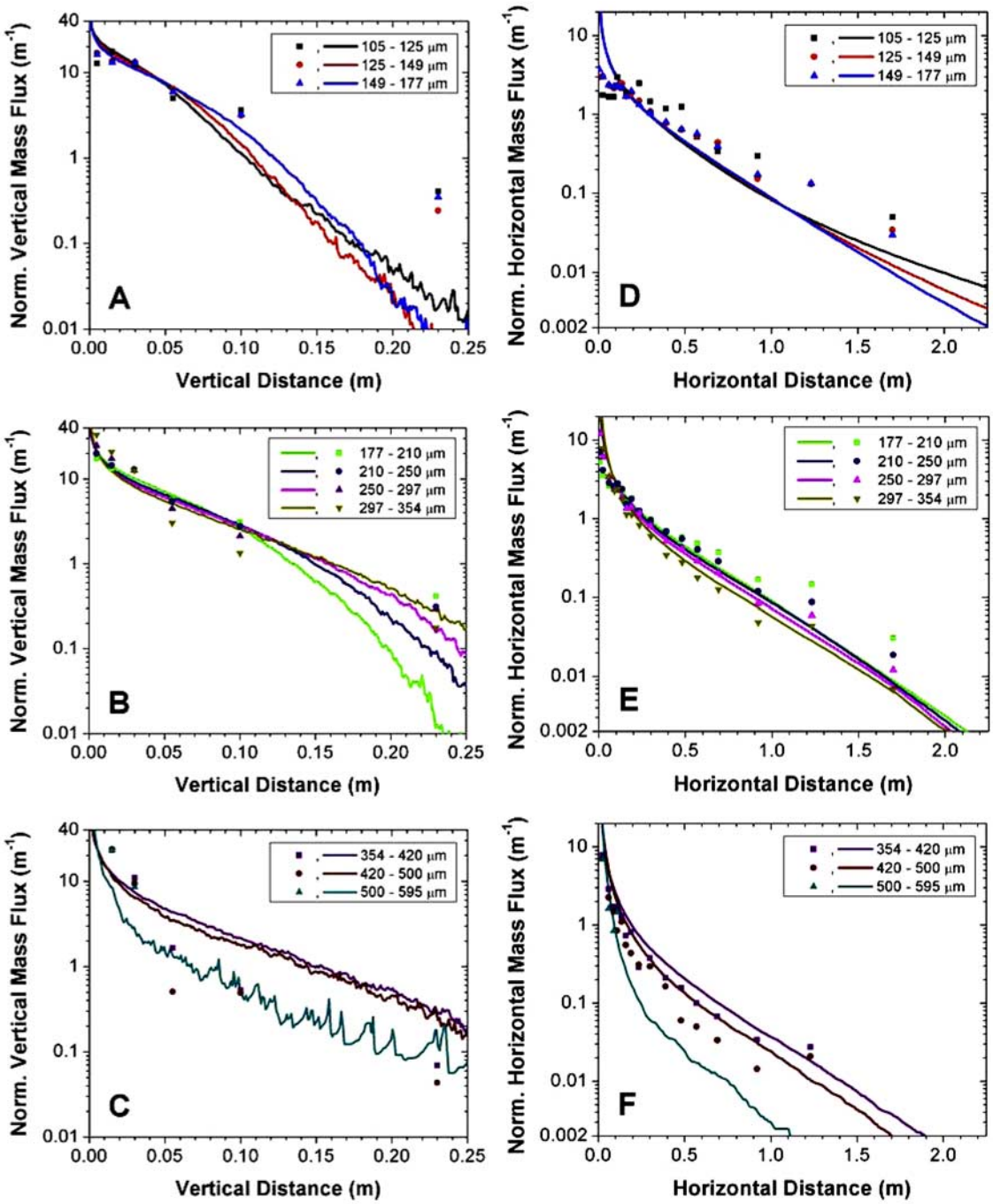

Figure 9. Vertical and horizontal mass flux profiles for different particle sizes. The colored symbols represent measurements taken at $u^* = 0.36$ m/s by *Namikas* [1999, 2003, 2006], and colored lines denote the model prediction for the corresponding particle size. In order to facilitate comparison, both measured and modeled mass flux profiles are normalized by the total saltation mass flux of a given particle bin. The increased noise at larger heights in the vertical mass flux profiles is due to the low probability of particles to saltate at those heights, which results in a larger uncertainty.

[47] Figure 9 compares modeled and measured horizontal and vertical mass flux profiles of particles of various sizes [*Namikas*, 2006]. There is reasonable to good agreement between measurements and the predictions of our model, especially when the many uncertainties that affect the results are considered. The predicted flux of fine particles ($\lesssim$200 μm) does however decay somewhat too quickly with vertical and horizontal distances (Figures 9a and 9d). These particles are substantially affected by turbulence [*Anderson*, 1987] and this discrepancy could thus be an indication that the modeled Lagrangian timescale (see section 2.1.2) is too short. Field measurements of this timescale in the saltation layer would therefore be a valuable addition to the literature.

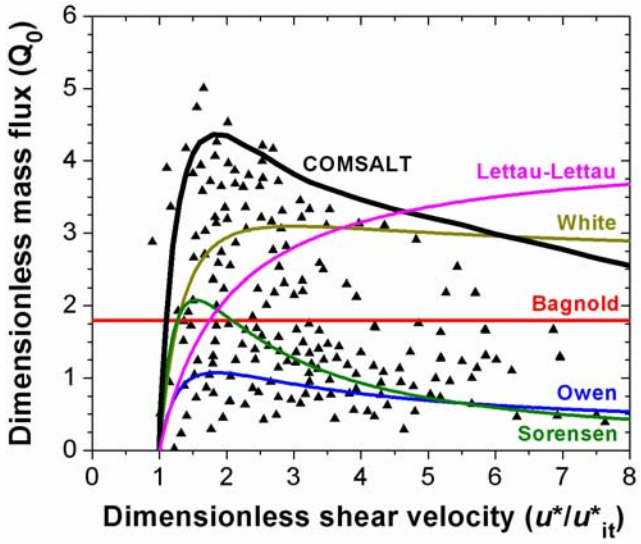

Figure 10. Dimensionless saltation mass flux Q_0 (see section 3.2) as a function of dimensionless shear velocity (u^*/u^*_{it}, where u^*_{it} is the impact threshold) simulated with our numerical model (black line), and compared with results from over a dozen wind tunnel studies and one field study compiled by *Iversen and Rasmussen* [1999] (triangles). The large scatter in the experimental results is likely caused by varying experimental conditions, such as particle size, air pressure, and wind tunnel characteristics [*Iversen and Rasmussen*, 1999]. A peak in the dimensionless mass flux is nonetheless apparent around $u^*/u^*_{\mathrm{it}} \approx 2$, and is reproduced by the model. For comparison we also included prominent empirical equations of the saltation mass flux (colored lines) by *Bagnold* [1941] ($Q_0 = 1.8$), *Owen* [1964] ($Q_0 = [0.25 + v_t/3u^*]\lfloor 1 - (u^*_{it}/u^*)^2 \rfloor$, where v_t is the terminal velocity of saltating particles), *Lettau and Lettau* [1978] ($Q_0 = 4.2[1 - u^*_{it}/u^*]$), *White* [1979] ($Q_0 = 2.61[1 - u^*_{it}/u^*][1 + u^*_{it}/u^*]^2$), and *Sorensen* [1991, 2004] ($Q_0 = [1 - u^{*2}_{it}/u^{*2}][\alpha + \gamma u^*_{it}/u^* + \beta u^{*2}_{it}/u^{*2}]$, with $\alpha = 0$, $\beta = 3.9$, and $\gamma = 3.0$ from *Sorensen* [2004, Figure 3]). Model results (black line) were obtained for the size distribution of typical beach sand reported by *Namikas* [2003], with an approximate median diameter of 250 μm. For very large shear velocities (i.e., $u^*/u^*_{\mathrm{it}} > \sim 4$), a substantial fraction (on the order of 5–25%) of the predicted mass flux is due to suspended sand transported at large heights. To exclude this fraction from the saltation mass flux, we omit the mass flux transported above a height of 0.5 m, in accordance with the vertical extent of mass flux collectors used in wind tunnel [e.g., *Iversen and Rasmussen*, 1999] and field studies [e.g., *Bagnold*, 1938; *Greeley et al.*, 1996; *Namikas*, 2003].

[48] Another possible explanation for this discrepancy could be that smaller particles rebound with a greater fraction of their inbound kinetic energy than larger particles do. Indeed, *Namikas* [2006] recently proposed that particles leave the surface with a kinetic energy that is independent of particle size. A semiempirical numerical model using this assumption showed excellent agreement with measurements [*Namikas*, 2006]. While there is evidence for Namikas' hypothesis from experiments with ice particles [e.g., *Higa et al.*, 1998], the laboratory experiments of Rice, Willets, and coworkers [*Willetts and Rice*, 1985, 1986, 1989; *Rice et al.*, 1995, 1996] found no evidence of a dependence of the restitution coefficient (i.e., the fraction of the impact speed retained by the rebounding particle) on particle size. Another concern is that Namikas' model requires the speed of small particles leaving the surface to be several times their terminal speed, which would imply that these particles gain energy upon rebounding from the surface, which is energetically inconsistent. While it thus seems unlikely that Namikas' hypothesis of a constant rebounding kinetic energy is correct in the strictest sense, the notion that the restitution coefficient increases with decreasing particle size is intriguing and deserving of further experimentation. Indeed, indirect evidence of this hypothesis is COMSALT's underestimation of the mass flux at larger heights for small particles (Figure 9).

3.2. Height-Integrated Mass Flux

[49] The total height-integrated mass flux of saltating particles is a key parameter for studies of dune formation [*Sauermann et al.*, 2001], wind erosion [*Sterk*, 2003], and dust aerosol emission [*Marticorena and Bergametti*, 1995]. Many wind tunnel and field measurements have therefore measured the variation of the total mass flux with shear velocity. These measurements are however difficult to compare directly because of variations in experimental conditions, such as particle size, wind tunnel characteristics, and air pressure. To nonetheless make a comparison between the large body of experimental studies of saltation mass flux and our model predictions, we nondimensionalize the total mass flux [*Iversen and Rasmussen*, 1999],

$$Q_0 = \frac{gQ}{\rho_a u^{*3}}, \tag{33}$$

where Q is the total height-integrated saltation mass flux, which is usually assumed to scale with the cube of the shear velocity [*Bagnold*, 1941; *Owen*, 1964; *Iversen and Rasmussen*, 1999].

[50] Figure 10 compares our model predictions to a compilation of field and wind tunnel measurements of the dimensionless mass flux [*Iversen and Rasmussen*, 1999]. Our model reproduces the observed peak of the dimensionless mass flux at $u^*/u^*_{\mathrm{it}} \approx 2$ [*Iversen and Rasmussen*, 1999], where u^*_{it} is the impact threshold, as well as the subsequent decrease for larger shear velocities. Many empirical models are unable to reproduce these features (see Figure 10 and *Iversen and Rasmussen* [1999]). The predicted height-integrated mass flux does appear larger than reported by most experimental studies, which is at least partially because sand collectors used in these studies have an efficiency of only ~50–70% [*Greeley et al.*, 1996; *Rasmussen and Mikkelsen*, 1998]. Moreover, both midair collisions and strong electrostatic forces are hypothesized to decrease the mass flux at large shear velocities [*Sorensen and McEwan*, 1996; *Sorensen*, 2004; *Kok and Renno*, 2008]. Since both these processes are not included in the present model version, the overestimation of the mass flux at large shear velocities is not surprising.

3.3. Size Distribution of Saltating Particles

[51] Once saltation is initiated, the transfer of momentum to the soil bed by particle impacts causes a wide range of

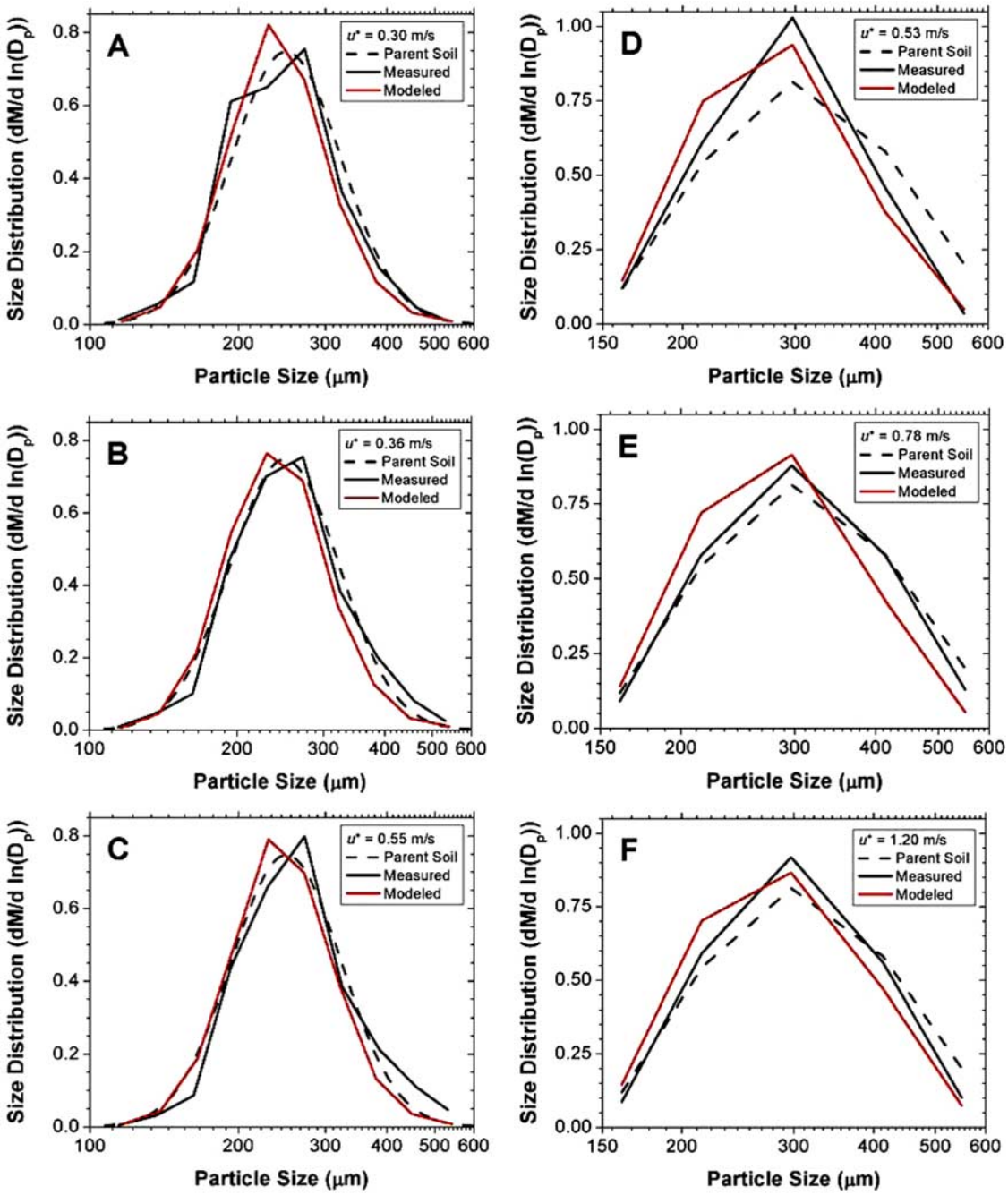

Figure 11. Size distributions of saltating particles during saltation, as measured (solid black lines) by (left) *Namikas* [1999, 2003, 2006] and (right) *Williams* [1964] and simulated by COMSALT (red solid lines). Model results were obtained for the same parent soil (dashed black lines) and wind conditions. The saltation size distribution for Namikas' field measurements was obtained by summing the particle size-resolved vertical mass flux reported in Figure 3 of *Namikas* [2006]. We define the size distribution of saltating particles as the contribution of each particle bin to the total height-integrated mass flux, in accordance with measurements [*Williams*, 1964; *Namikas*, 2006].

particle sizes to enter saltation. Thus saltation is not limited to those particles whose threshold shear velocity (u_t^*) is below the wind shear velocity (u^*), as is often assumed. Rather, the size distribution of saltating particles is determined by two factors: (1) the probability of particles of a given size to be ejected from the surface (see equation (25)) and (2) the time that particles of a given size spend in saltation before settling back onto the soil surface.

[52] Wind tunnel measurements of the size distribution of saltating particles were reported by *Williams* [1964]. Moreover, we used the size-resolved vertical mass flux profiles reported by *Namikas* [2006] to obtain the saltation size

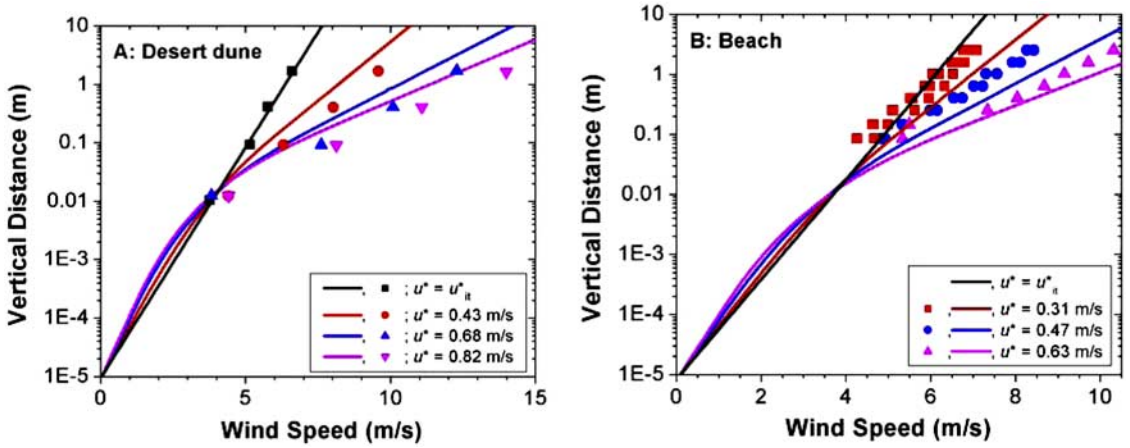

Figure 12. Wind profiles during saltation on a desert dune [*Bagnold*, 1938] (symbols in the left graph), on a beach [*Namikas*, 1999] (symbols in the right graph), and modeled (colored lines) for similar conditions. Since *Bagnold* [1938] did not report a soil size distribution, we assume this to be similar to the size distribution of saltating particles (i.e., we used the saltating particle size distribution for $u^* = 0.33$ m/s reported in Bagnold's Figure 7), as experiments indicate (see Figure 11). Using this size distribution, the model predicts an impact threshold (black line) that is in excellent agreement with Bagnold's measured impact threshold (black squares). The model results for *Namikas* [1999] use the size distribution as reported by *Namikas* [2003], for which the model predicts an impact threshold of 0.21 m/s (black line), in good agreement with Namikas' estimated impact threshold of 0.20–0.23 m/s [*Namikas*, 1999].

distribution in his field measurements [*Namikas*, 1999, 2003]. The model-predicted saltation size distribution shows good agreement with the measurements of *Williams* [1964] and with those reconstructed from *Namikas* [2006] (Figure 11). In general, we find that the size distribution of saltating particles in the range 100–500 μm roughly matches the parent soil size distribution [*Kok and Renno*, 2008]. This occurs because while larger particles have an increased chance of being ejected from the surface (see equation (25) and *Rice et al.* [1995]), they also tend to have shorter lifetimes. Conversely, smaller particles are ejected less frequently but have longer lifetimes once ejected. These two effects cause the saltation size distribution to be similar to that of the soil in the range 100–500 μm.

[53] Note that both measurements and our model predictions show that the size distribution shifts slightly toward larger particles as the shear velocity increases. The likely physical reason for this phenomenon is that, while the average impact speed stays approximately constant with increasing shear velocity (see discussion in section 2.4), we find that the probability distribution of impact speeds broadens with shear velocity. As a result, an increasing fraction of impacting particles has very large impact speeds. Since larger surface particles require greater impact speeds to be splashed into saltation, rather than creep along the surface, the number of large particles entering saltation increases with shear velocity. This leads to the observed and predicted slight shift in the saltation size distribution toward larger particle sizes as the shear velocity increases.

3.4. Wind Speed and Roughness Length in Saltation

[54] Measurements of the wind speed in saltation were made by numerous researchers and are summarized by *Sherman and Farrell* [2008]. Figure 12 shows wind speeds predicted by our model and compared to wind speeds measured on a desert dune by *Bagnold* [1938] and on a beach by *Namikas* [1999]. The model is in reasonable agreement in both cases but underestimates the wind speed in comparison with *Bagnold* [1938], while it overestimates the wind speed in comparison with *Namikas* [1999]. Note that the focusing of the wind profiles (the so-called "Bagnold focus" [*Bagnold*, 1936]) at a height of $\sim$1 cm is reproduced in both cases.

[55] At a given shear velocity, the wind speed directly above the saltation layer is determined by the increase in the aerodynamic roughness length produced by the transfer of wind momentum to saltating particles [*Owen*, 1964]. Several models have been proposed to relate the aerodynamic roughness length in saltation to the shear velocity [*Charnock*, 1955; *Raupach*, 1991; *Sherman*, 1992]. However, the most physically plausible relationship is probably the modified Charnock relationship [*Sherman*, 1992; *Sherman and Farrell*, 2008]

$$z_{0S} = z_0 + C_m \frac{(u^* - u^*_{it})^2}{g}, \tag{34}$$

where z_{0S} is the aerodynamic roughness length during saltation and u^*_{it} is the impact threshold. *Sherman and Farrell* [2008] used a compilation of 137 wind profiles from field measurements and determined the value of the modified Charnock constant to be $C_m = 0.132 \pm 0.080$. However, for a compilation of 197 wind tunnel experiments, they found that $C_m = 0.0120 \pm 0.0007$. This significant difference in the saltation roughness length between field and wind tunnel experiments indicates that most wind tunnel experiments do not successfully replicate the physics of natural saltation [*Sherman and Farrell*, 2008]. A similar result was obtained by *Farrell and Sherman* [2006], who

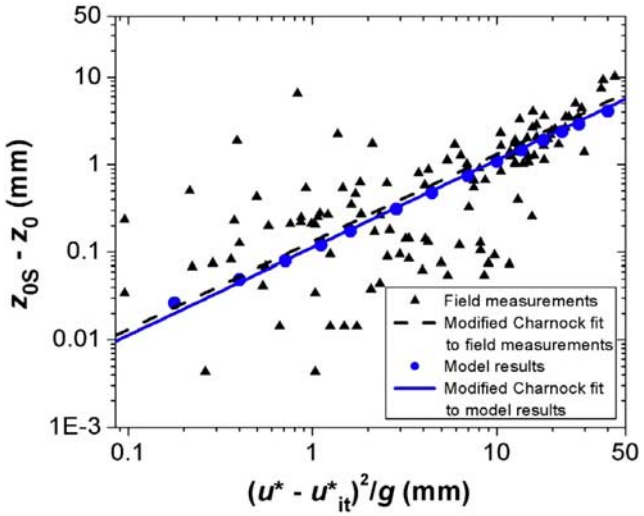

Figure 13. Aerodynamic roughness length in saltation from a compilation of field measurements by *Sherman and Farrell* [2008] (black triangles) and simulated by our model (blue circles). Also included are fits with the modified Charnock relationship (equation (34)) [*Charnock*, 1955; *Sherman*, 1992] to the compilation of field measurements (black dashed line) and to our model results (blue solid line). The large scatter in the experimental results is probably due to measurement error and variations in experimental conditions, such as particle size, soil moisture content, and surface slope.

reported that vertical mass flux profiles in wind tunnel experiments are significantly different from those occurring in natural saltation.

[56] Figure 13 compares the model-predicted saltation roughness length with a collection of field measurements compiled by *Sherman and Farrell* [2008]. Our model reproduces the functional form of the modified Charnock model [*Sherman*, 1992] very well, while the agreement with alternative models, such as the Raupach model [*Raupach*, 1991] and the normal Charnock model [*Charnock*, 1955], is not as good (not shown). Moreover, the best fit value of the modified Charnock constant from our model results is $C_m = 0.118$, which is very close to the value obtained by *Sherman and Farrell* [2008]. Our results are thus in excellent agreement with field measurements of the roughness length in saltation and provide strong support for the physical correctness of the modified Charnock relationship [*Sherman*, 1992; *Sherman and Farrell*, 2008].

4. Conclusions

[57] We have developed the most comprehensive numerical model of steady state saltation to date (COMSALT). Our model explicitly simulates particle trajectories due to gravitational and fluid forces and accounts for the effects of turbulence using a parameterization that shows good agreement with measurements (Figure 3). COMSALT also includes a novel physically based parameterization of the splashing of surface particles by impacting saltating particles. This parameterization shows good agreement with available measurements (Figure 6), correctly predicts the average impact speed of particles in steady state saltation (section 2.4) and, when implemented in our numerical saltation model, reproduces measurements of the impact threshold (Figure 7). COMSALT uses a minimum of empirical relations, which makes it suitable for a straightforward adaptation to similar problems in different physical regimes, such as saltating snow, saltation on different planets, and saltation in water. COMSALT was coded in MATLAB and is freely available by contacting the first author (J.K.).

[58] While previous numerical models have been able to reproduce certain measurements of natural saltation, COMSALT is the first physically based model that can reproduce a wide variety of experimental data, including vertical and horizontal profiles of particle mass flux (Figures 8 and 9), the total height-integrated mass flux (Figure 10), the size distribution of saltating particles (Figure 11), and the wind speed and aerodynamic roughness length in saltation (Figures 12 and 13).

[59] At large shear velocities, there seems to be less agreement between model predictions and measurements of the vertical profile of the mass flux and the total mass flux (Figures 8c and 10). This might occur because the current model version neglects midair collisions and electrostatic forces, which are both thought to become important at large shear velocities [*Sorensen and McEwan*, 1996; *Kok and Renno*, 2006, 2008]. Work is in progress to include these processes in a future model version (Kok and Renno, manuscript in preparation, 2009).

[60] A detailed understanding of saltation is vital to a variety of problems across scientific disciplines. Of particular interest is the formation of sand dunes and the emission of dust aerosols by the impacts of saltating particles on the soil surface [*Shao et al.*, 1993; *Marticorena and Bergametti*, 1995; *Shao*, 2000]. The ability of COMSALT to reproduce natural saltation makes it a potentially valuable resource in advancing our understanding of these critical processes.

[61] **Acknowledgments.** We thank Steven Namikas and Keld Rasmussen for insightful discussions, Eugene Farrell for providing us with his compilation of aerodynamic roughness lengths, and Shanna Shaked and three anonymous reviewers for comments on the manuscript. This research was supported by NSF award ATM 0622539 and by a Rackham Predoctoral Fellowship to J.K.

References

Almeida, M. P., et al. (2006), Aeolian transport layer, *Phys. Rev. Lett.*, *96*(1), 018001, doi:10.1103/PhysRevLett.96.018001.

Almeida, M. P., et al. (2008), Giant saltation on Mars, *Proc. Natl. Acad. Sci. U. S. A.*, *105*(17), 6222–6226, doi:10.1073/pnas.0800202105.

Anderson, R. S. (1987), Eolian sediment transport as a stochastic process–The effects of a fluctuating wind on particle trajectories, *J. Geol.*, *95*(4), 497–512.

Anderson, R. S., and P. K. Haff (1988), Simulation of eolian saltation, *Science*, *241*(4867), 820–823, doi:10.1126/science.241.4867.820.

Anderson, R. S., and P. K. Haff (1991), Wind modification and bed response during saltation of sand in air, *Acta Mech.*, *1*, 21–51.

Anderson, R. S., and B. Hallet (1986), Sediment transport by wind—Toward a general model, *Geol. Soc. Am. Bull.*, *97*(5), 523–535, doi:10.1130/0016-7606(1986)97<523:STBWTA>2.0.CO;2.

Andreotti, B. (2004), A two-species model of aeolian sand transport, *J. Fluid Mech.*, *510*, 47–70, doi:10.1017/S0022112004009073.

Anfossi, D., et al. (2006), Estimation of the ratio between the Lagranglan and Eulerian time scales in an atmospheric boundary layer generated by large eddy simulation, *Atmos. Environ.*, *40*(2), 326–337, doi:10.1016/j.atmosenv.2005.09.041.

Bagnold, R. A. (1936), The movement of desert sand, *Proc. R. Soc. London A*, *157*, 594–620.
Bagnold, R. A. (1937), The transport of sand by wind, *Geogr. J.*, *89*(5), 409–438, doi:10.2307/1786411.
Bagnold, R. A. (1938), The measurement of sand storms, *Proc. R. Soc. London A*, *167*, 282–291.
Bagnold, R. A. (1941), *The Physics of Blown Sand and Desert Dunes*, Methuen, New York.
Bagnold, R. A. (1973), Nature of saltation and bed-load transport in water, *Proc. R. Soc. London A*, *332*, 473–504.
Beladjine, D., et al. (2007), Collision process between an incident bead and a three-dimensional granular packing, *Phys. Rev. E*, *75*(6), 061305, doi:10.1103/PhysRevE.75.061305.
Camenen, B. (2007), Simple and general formula for the settling velocity of particles, *J. Hydraul. Eng.*, *133*(2), 229–233, doi:10.1061/(ASCE)0733-9429(2007)133:2(229).
Charnock, H. (1955), Wind stress on a water surface, *Q. J. R. Meteorol. Soc.*, *81*, 639–640, doi:10.1002/qj.49708135027.
Cheng, N. S. (1997), Simplified settling velocity formula for sediment particle, *J. Hydraul. Eng.*, *123*(2), 149–152, doi:10.1061/(ASCE)0733-9429(1997)123:2(149).
Chepil, W. S., and N. P. Woodruff (1963), The physics of wind erosion and its control, *Adv. Agron.*, *15*, 211–302, doi:10.1016/S0065-2113(08)60400-9.
Creyssels, M., et al. (2009), Saltating particles in a turbulent boundary layer: Experiment and theory, *J. Fluid Mech.*, *625*, 47–74, doi:10.1017/S0022112008005491.
Csanady, G. T. (1963), Turbulent diffusion of heavy particles in the atmosphere, *J. Atmos. Sci.*, *20*(3), 201–208, doi:10.1175/1520-0469(1963)020<0201:TDOHPI>2.0.CO;2.
Dietrich, W. E. (1982), Settling velocity of natural particles, *Water Resour. Res.*, *18*(6), 1615–1626, doi:10.1029/WR018i006p01615.
Dong, Z., N. Huang, and X. Liu (2005), Simulation of the probability of midair interparticle collisions in an aeolian saltating cloud, *J. Geophys. Res.*, *110*, D24113, doi:10.1029/2005JD006070.
Farrell, E. J., and D. J. Sherman (2006), Process-scaling issues for aeolian transport modelling in field and wind tunnel experiments: Roughness length and mass flux distributions, *J. Coastal Res.*, *1*, 384–389.
Fenton, L. K., et al. (2007), Global warming and climate forcing by recent albedo changes on Mars, *Nature*, *446*(7136), 646–649, doi:10.1038/nature05718.
Goudie, A. S., and N. J. Middleton (2006), *Desert Dust in the Global System*, Springer, Berlin.
Greeley, R., and J. D. Iversen (1985), *Wind as a Geological Process on Earth, Mars, Venus, and Titan*, Cambridge Univ. Press, New York.
Greeley, R., et al. (1996), Field measurements of the flux and speed of wind-blown sand, *Sedimentology*, *43*(1), 41–52, doi:10.1111/j.1365-3091.1996.tb01458.x.
Haff, P. K., and R. S. Anderson (1993), Grain scale simulations of loose sedimentary beds–The example of grain-bed impacts in aeolian saltation, *Sedimentology*, *40*(2), 175–198, doi:10.1111/j.1365-3091.1993.tb01760.x.
Hairer, E., S. P. Nørsett, and G. Wanner (1993), *Solving Ordinary Differential Equations I: Nonstiff Problems*, 2nd ed., Springer, Berlin.
Higa, M., M. Arakawa, and N. Maeno (1998), Size dependence of restitution coefficients of ice in relation to collision strength, *Icarus*, *133*, 310–320, doi:10.1006/icar.1998.5938.
Huang, N., Y. Zhang, and R. D'Adamo (2007), A model of the trajectories and midair collision probabilities of sand particles in a steady state saltation cloud, *J. Geophys. Res.*, *112*, D08206, doi:10.1029/2006JD007480.
Huang, N., F. Shi, and R. S. Van Pelt (2008), The effects of slope and slope position on local and upstream fluid threshold friction velocities, *Earth Surf. Processes Landforms*, *33*, 1814–1823, doi:10.1002/esp.1735.
Hunt, J. C. R., and P. Nalpanis (1985), Saltating and suspended particles over flat and sloping surfaces. 1. Modelling concepts, in *Proceedings of the International Workshop on the Physics of Blown Sand*, edited by O. E. Barndorff-Nielsen, pp. 9–36, Univ. of Aarhus, Aarhus, Denmark.
Hunt, J. C. R., and A. H. Weber (1979), Lagrangian statistical analysis of diffusion from a ground-level source in a turbulent boundary-layer, *Q. J. R. Meteorol. Soc.*, *105*(444), 423–443, doi:10.1002/qj.49710544407.
Iversen, J. D., and K. R. Rasmussen (1994), The effect of surface slope on saltation threshold, *Sedimentology*, *41*(4), 721–728, doi:10.1111/j.1365-3091.1994.tb01419.x.
Iversen, J. D., and K. R. Rasmussen (1999), The effect of wind speed and bed slope on sand transport, *Sedimentology*, *46*(4), 723–731, doi:10.1046/j.1365-3091.1999.00245.x.
Jackson, D. W. T., and J. McCloskey (1997), Preliminary results from a field investigation of aeolian sand transport using high resolution wind and transport measurements, *Geophys. Res. Lett.*, *24*(2), 163–166, doi:10.1029/96GL03967.
Jickells, T. D., et al. (2005), Global iron connections between desert dust, ocean biogeochemistry, and climate, *Science*, *308*(5718), 67–71, doi:10.1126/science.1105959.
Kang, L. Q., et al. (2008), Reconstructing the vertical distribution of the aeolian saltation mass flux based on the probability distribution of lift-off velocity, *Geomorphology*, *96*(1–2), 1–15, doi:10.1016/j.geomorph.2007.07.005.
Kok, J. F., and D. J. Lacks (2009), Electrification of granular systems of identical insulators, *Phys. Rev. E*, *79*(5), 051304, doi:10.1103/PhysRevE.79.051304.
Kok, J. F., and N. O. Renno (2006), Enhancement of the emission of mineral dust aerosols by electric forces, *Geophys. Res. Lett.*, *33*, L19S10, doi:10.1029/2006GL026284.
Kok, J. F., and N. O. Renno (2008), Electrostatics in wind-blown sand, *Phys. Rev. Lett.*, *100*(1), 014501, doi:10.1103/PhysRevLett.100.014501.
Kok, J. F., and N. O. Renno (2009), The electrification of wind-blown sand on Mars and its implications for atmospheric chemistry, *Geophys. Res. Lett.*, *36*, L05202, doi:10.1029/2008GL036691.
Lettau, K., and H. H. Lettau (1978), Experimental and micro-meteorological field studies of dune migration, in *Exploring the World's Driest Climate, Rep. 101*, edited by H. H. Lettau and K. Lettau, pp. 110–147, Inst. for Environ. Stud., Univ. of Wisc., Madison.
Leuning, R., et al. (2000), Source/sink distributions of heat, water vapour, carbon dioxide and methane in a rice canopy estimated using Lagrangian dispersion analysis, *Agric. For. Meteorol.*, *104*(3), 233–249, doi:10.1016/S0168-1923(00)00158-1.
Loth, E. (2008), Lift of a solid spherical particle subject to vorticity and/or spin, *AIAA J.*, *46*(4), 801–809, doi:10.2514/1.29159.
Marticorena, B., and G. Bergametti (1995), Modeling the atmospheric dust cycle: 1. Design of a soil-derived dust emission scheme, *J. Geophys. Res.*, *100*(D8), 16,415–16,430, doi:10.1029/95JD00690.
McEwan, I. K., and B. B. Willetts (1991), Numerical model of the saltation cloud, *Acta Mech.*, *1*, 53–66.
McEwan, I. K., and B. B. Willetts (1993), Adaptation of the near-surface wind to the development of sand transport, *J. Fluid Mech.*, *252*, 99–115, doi:10.1017/S0022112093003684.
McLaughlin, J. B. (1991), Inertial migration of a small sphere in linear shear flows, *J. Fluid Mech.*, *224*, 261–274, doi:10.1017/S0022112091001751.
Mitha, S., et al. (1986), The grain-bed impact process in aeolian saltation, *Acta Mech.*, *63*(1–4), 267–278, doi:10.1007/BF01182553.
Nalpanis, J., J. C. R. Hunt, and C. F. Barrett (1993), Saltating particles over flat beds, *J. Fluid Mech.*, *251*, 661–685, doi:10.1017/S0022112093003568.
Namikas, S. L. (1999), Aeolian saltation: Field measurements and numerical simulations, Ph.D. thesis, Univ. of South. Calif., Los Angeles.
Namikas, S. L. (2003), Field measurement and numerical modelling of aeolian mass flux distributions on a sandy beach, *Sedimentology*, *50*(2), 303–326, doi:10.1046/j.1365-3091.2003.00556.x.
Namikas, S. L. (2006), A conceptual model of energy partitioning in the collision of saltating grains with an unconsolidated sediment bed, *J. Coastal Res.*, *22*(5), 1250–1259, doi:10.2112/06A-0007.1.
Nemoto, M., and K. Nishimura (2004), Numerical simulation of snow saltation and suspension in a turbulent boundary layer, *J. Geophys. Res.*, *109*, D18206, doi:10.1029/2004JD004657.
Nikuradse, J. (1933), Laws of flow in rough pipes (1950 translation), *Tech. Memo. 1292*, Natl. Advis. Comm. on Aeronaut., Washington, D. C.
Nishimura, K., and J. C. R. Hunt (2000), Saltation and incipient suspension above a flat particle bed below a turbulent boundary layer, *J. Fluid Mech.*, *417*, 77–102, doi:10.1017/S0022112000001014.
Oger, L., et al. (2005), Discrete element method studies of the collision of one rapid sphere on 2D and 3D packings, *Eur. Phys. J. E*, *17*(4), 467–476, doi:10.1140/epje/i2005-10022-x.
Owen, P. R. (1964), Saltation of uniform grains in air, *J. Fluid Mech.*, *20*(2), 225–242, doi:10.1017/S0022112064001173.
Prandtl, L. (1935), The mechanics of viscous flows, in *Aerodynamic Theory*, vol. III, edited by W. F. Durand, pp. 34–208, Springer, Berlin.
Rasmussen, K. R., and H. E. Mikkelsen (1998), On the efficiency of vertical array aeolian field traps, *Sedimentology*, *45*(4), 789–800, doi:10.1046/j.1365-3091.1998.00179.x.
Rasmussen, K. R., and M. Sorensen (2008), Vertical variation of particle speed and flux density in aeolian saltation: Measurement and modeling, *J. Geophys. Res.*, *113*, F02S12, doi:10.1029/2007JF000774.
Raupach, M. R. (1991), Saltation layers, vegetation canopies and roughness lengths, *Acta Mech.*, *1*, 83–96.
Raupach, M. R., et al. (1996), Coherent eddies and turbulence in vegetation canopies: The mixing-layer analogy, *Boundary Layer Meteorol.*, *78*(3–4), 351–382, doi:10.1007/BF00120941.

Renno, N. O., and J. F. Kok (2008), Electrical activity and dust lifting on Earth, Mars, and beyond, *Space Sci. Rev.*, *137*(1–4), 419–434, doi:10.1007/s11214-008-9377-5.

Renno, N. O., et al. (2004), MATADOR 2002: A pilot field experiment on convective plumes and dust devils, *J. Geophys. Res.*, *109*, E07001, doi:10.1029/2003JE002219.

Reynolds, A. M. (2000), On the formulation of Lagrangian stochastic models for heavy-particle trajectories, *J. Colloid Interface Sci.*, *232*(2), 260–268, doi:10.1006/jcis.2000.7208.

Rice, M. A., et al. (1995), An experimental study of multiple grain-size ejecta produced by collisions of saltating grains with a flat bed, *Sedimentology*, *42*(4), 695–706, doi:10.1111/j.1365-3091.1995.tb00401.x.

Rice, M. A., et al. (1996), Observations of collisions of saltating grains with a granular bed from high-speed cine-film, *Sedimentology*, *43*(1), 21–31, doi:10.1111/j.1365-3091.1996.tb01456.x.

Rioual, F., et al. (2000), Experimental study of the collision process of a grain on a two-dimensional granular bed, *Phys. Rev. E*, *62*(2), 2450–2459, doi:10.1103/PhysRevE.62.2450.

Rubinow, S. I., and J. B. Keller (1961), The transverse force on spinning spheres moving in a viscous liquid, *J. Fluid Mech.*, *11*(3), 447–459, doi:10.1017/S0022112061000640.

Saffman, P. G. (1965), The lift on a small sphere in a slow shear flow, *J. Fluid Mech.*, *22*(2), 385–400, doi:10.1017/S0022112065000824.

Saffman, P. G. (1968), Correction, *J. Fluid Mech.*, *31*, 624.

Sauermann, G., et al. (2001), Continuum saltation model for sand dunes, *Phys. Rev. E*, *64*(3), 031305, doi:10.1103/PhysRevE.64.031305.

Sawford, B. L., and F. M. Guest (1991), Lagrangian statistical simulation of the turbulent motion of heavy particles, *Boundary Layer Meteorol.*, *54*(1–2), 147–166, doi:10.1007/BF00119417.

Shao, Y. P. (1995), A Lagrangian stochastic model for nonpassive particle diffusion in turbulent flows, *Math. Comput. Model.*, *21*(9), 31–37, doi:10.1016/0895-7177(95)00049-8.

Shao, Y. P. (2000), *Physics and Modelling of Wind Erosion*, Kluwer Acad., Dordrecht, Netherlands.

Shao, Y. P., and A. Li (1999), Numerical modelling of saltation in the atmospheric surface layer, *Boundary Layer Meteorol.*, *91*(2), 199–225, doi:10.1023/A:1001816013475.

Shao, Y. P., and H. Lu (2000), A simple expression for wind erosion threshold friction velocity, *J. Geophys. Res.*, *105*(D17), 22,437–22,443, doi:10.1029/2000JD900304.

Shao, Y. P., and M. Mikami (2005), Heterogeneous saltation: Theory, observation and comparison, *Boundary Layer Meteorol.*, *115*(3), 359–379, doi:10.1007/s10546-004-7089-2.

Shao, Y., and M. R. Raupach (1992), The overshoot and equilibration of saltation, *J. Geophys. Res.*, *97*(D18), 20,559–20,564.

Shao, Y., M. R. Raupach, and P. A. Findlater (1993), Effect of saltation bombardment on the entrainment of dust by wind, *J. Geophys. Res.*, *98*(D7), 12,719–12,726, doi:10.1029/93JD00396.

Sherman, D. J. (1992), An equilibrium relationship for shear velocity and apparent roughness length in aeolian saltation, *Geomorphology*, *5*(3–5), 419–431, doi:10.1016/0169-555X(92)90016-H.

Sherman, D. J., and E. J. Farrell (2008), Aerodynamic roughness lengths over movable beds: Comparison of wind tunnel and field data, *J. Geophys. Res.*, *113*, F02S08, doi:10.1029/2007JF000784.

Snyder, W. H., and J. L. Lumley (1971), Some measurements of particle velocity autocorrelation functions in a turbulent flow, *J. Fluid Mech.*, *48*(1), 41–71, doi:10.1017/S0022112071001460.

Sokolik, I. N., D. M. Winker, G. Bergametti, D. A. Gillette, G. Carmichael, Y. J. Kaufman, L. Gomes, L. Schuetz, and J. E. Penner (2001), Introduction to special section: Outstanding problems in quantifying the radiative impacts of mineral dust, *J. Geophys. Res.*, *106*(D16), 18,015–18,027, doi:10.1029/2000JD900498.

Sorensen, M. (1991), An analytic model of wind-blown sand transport, *Acta Mech.*, *1*, 67–81.

Sorensen, M. (2004), On the rate of aeolian transport, *Geomorphology*, *59*(1–4), 53–62, doi:10.1016/j.geomorph.2003.09.005.

Sorensen, M., and I. McEwan (1996), On the effect of mid-air collisions on aeolian saltation, *Sedimentology*, *43*(1), 65–76, doi:10.1111/j.1365-3091.1996.tb01460.x.

Sterk, G. (2003), Causes, consequences and control of wind erosion in Sahelian Africa: A review, *Land Degrad. Develop.*, *14*(1), 95–108, doi:10.1002/ldr.526.

Taniere, A., et al. (1997), On the behaviour of solid particles in a horizontal boundary layer with turbulence and saltation effects, *Exp. Fluids*, *23*(6), 463–471, doi:10.1007/s003480050136.

Ungar, J. E., and P. K. Haff (1987), Steady-state saltation in air, *Sedimentology*, *34*(2), 289–299, doi:10.1111/j.1365-3091.1987.tb00778.x.

Van Dop, H., et al. (1985), Random-walk models for particle displacements in inhomogeneous unsteady turbulent flows, *Phys. Fluids*, *28*(6), 1639–1653, doi:10.1063/1.864956.

Wang, D. W., et al. (2008), Statistical analysis of sand grain/bed collision process recorded by high-speed digital camera, *Sedimentology*, *55*(2), 461–470, doi:10.1111/j.1365-3091.2007.00909.x.

Werner, B. T. (1987), A physical model of wind-blown sand transport, Ph.D. thesis, Calif. Inst. of Technol., Pasadena.

Werner, B. T. (1990), A steady-state model of wind-blown sand transport, *J. Geol.*, *98*(1), 1–17.

White, B. R. (1979), Soil transport by winds on Mars, *J. Geophys. Res.*, *84*(B9), 4643–4651, doi:10.1029/JB084iB09p04643.

White, B. R. (1982), 2-phase measurements of saltating turbulent boundary-layer flow, *Int. J. Multiphase Flow*, *8*(5), 459–473, doi:10.1016/0301-9322(82)90018-0.

White, B. R., and J. C. Schulz (1977), Magnus effect in saltation, *J. Fluid Mech.*, *81*(3), 497–512, doi:10.1017/S0022112077002183.

Willetts, B. B., and M. A. Rice (1985), Inter-saltation collisions, in *Proceedings of the International Workshop on the Physics of Blown Sand*, edited by O. E. Barndorff-Nielsen, pp. 83–100, Univ. of Aarhus, Aarhus, Denmark.

Willetts, B. B., and M. A. Rice (1986), Collisions in aeolian saltation, *Acta Mech.*, *63*(1–4), 255–265, doi:10.1007/BF01182552.

Willetts, B. B., and M. A. Rice (1989), Collisions of quartz grains with a sand bed–the influence of incident angle, *Earth Surf. Processes Landforms*, *14*(8), 719–730, doi:10.1002/esp.3290140806.

Williams, G. (1964), Some aspects of the eolian saltation load, *Sedimentology*, *3*(4), 257–287, doi:10.1111/j.1365-3091.1964.tb00642.x.

Wilson, J. D., and B. L. Sawford (1996), Review of Lagrangian stochastic models for trajectories in the turbulent atmosphere, *Boundary Layer Meteorol.*, *78*(1–2), 191–210, doi:10.1007/BF00122492.

Xie, L., Y. Ling, and X. Zheng (2007), Laboratory measurement of saltating sand particles' angular velocities and simulation of its effect on saltation trajectory, *J. Geophys. Res.*, *112*, D12116, doi:10.1029/2006JD008254.

Yue, G. W., and X. J. Zheng (2006), Electric field in windblown sand flux with thermal diffusion, *J. Geophys. Res.*, *111*, D16106, doi:10.1029/2005JD006972.

Zheng, X. J., et al. (2006), The effect of electrostatic force on the evolution of sand saltation cloud, *Eur. Phys. J. E*, *19*(2), 129–138, doi:10.1140/epje/e2006-00020-9.

Zou, X. Y., et al. (2007), Effects of the Magnus and Saffman forces on the saltation trajectories of sand grain, *Geomorphology*, *90*(1–2), 11–22, doi:10.1016/j.geomorph.2007.01.006.

J. F. Kok and N. O. Renno, Applied Physics Program, University of Michigan, Ann Arbor, MI 48109, USA. (jfkok@umich.edu)